INL/JOU-18-52239-Revision-0

Postirradiation Examination of FUTURIX-FTA metallic alloy experiments

Jason M Harp, Luca Capriotti, Heather J MacLean Chichester

January 2019

The INL is a U.S. Department of Energy National Laboratory
operated by Battelle Energy Alliance

INL/JOU-18-52239-Revision-0

Postirradiation Examination of FUTURIX-FTA metallic alloy experiments

Jason M Harp, Luca Capriotti, Heather J MacLean Chichester

January 2019

Idaho National Laboratory
Idaho Falls, Idaho 83415

http://www.inl.gov

Prepared for the
U.S. Department of Energy

Under DOE Idaho Operations Office
Contract DE-AC07-05ID14517

Accepted Manuscript

Postirradiation Examination of FUTURIX-FTA metallic alloy experiments

Jason M. Harp, Luca Capriotti, Heather J.M. Chichester

PII: S0022-3115(18)31376-X

DOI: https://doi.org/10.1016/j.jnucmat.2018.12.051

Reference: NUMA 51383

To appear in: *Journal of Nuclear Materials*

Received Date: 8 October 2018

Revised Date: 6 December 2018

Accepted Date: 31 December 2018

Please cite this article as: J.M. Harp, L. Capriotti, H.J.M. Chichester, Postirradiation Examination of FUTURIX-FTA metallic alloy experiments, *Journal of Nuclear Materials* (2019), doi: https://doi.org/10.1016/j.jnucmat.2018.12.051.

Postirradiation Examination of FUTURIX-FTA metallic alloy experiments

Jason M. Harp*, Luca Capriotti, Heather J.M. Chichester
Idaho National Laboratory
PO Box 1625, Idaho Falls, ID, USA 83415
*Corresponding article jason.harp@inl.gov

Abstract

Two different metallic nuclear fuel alloys intended for transmutation applications in fast neutron spectrum nuclear reactors have been irradiated, and their performance has been evaluated after irradiation. These alloys contained elevated levels of plutonium and other minor actinides (Am, Np) compared to historically irradiated fast reactor fuel to ascertain the impact of these isotopes on fuel performance. The irradiation of these alloys was performed at the Phénix fast reactor in France to facilitate comparisons between true fast spectrum irradiations and pseudo-fast spectrum irradiations performed at the thermal neutron spectrum Idaho National Laboratory Advanced Test Reactor. The irradiation tests were designated FUTURIX-FTA DOE1 which contained a low-fertile alloy and FUTURIX-FTA DOE2 which contained a non-fertile alloy. The DOE1 fuel was irradiated to a measured burnup of 9.5 % fissions per initial heavy metal atom (FIMA), and the DOE2 fuel was irradiated to a measured burnup of 12.7 % fissions per initial heavy metal atom. This work reports baseline Postirradiation Examination (PIE) results for DOE1 and DOE2. Fuel swelling, fission product distribution, cladding strain, fission gas release, fuel microstructure, fuel cladding chemical interaction and minor actinide transmutation were all evaluated. Cladding strain was negligible and fission gas release was 52% for DOE1 and 69% for DOE2. The exams show the 2 pins behaved very similar to EBR-II metallic fuel experience. Minor actinides seem to not affect the performance of this candidate transmutation fuel. Performance data from these irradiations can be used to inform the feasibility of minor actinide transmutation in future reactor systems.

Keywords:

Postirradiation Examination, Metallic fuel, Transmutation Fuel, FUTURIX-FTA

Highlights:

- The FUTURIX-FTA experiment demonstrated potential alloys for minor actinide transmutation
- Performance of FUTURIX-FTA metallic fuel is in line with historical experience from other fast reactors such as EBR-II.

1. Introduction

The destruction of long lived minor actinide isotopes generated in irradiated nuclear fuel by transmutation in fast reactors is a goal of the US DOE Nuclear Technology Research & Development program. The purpose of proposed transmutation fuel forms is reduction of the radio-toxicity of future high level waste destined for disposal in geologic repositories. The objective, then, of transmutation fuel development is a demonstrated fuel concept that accomplishes transmutation while meeting the fuel performance requirements of the reactor [1,2]. The FUTURIX-FTA irradiation was a joint collaboration between the Department of Energy (DOE) in the U.S. and the Commissariat à l'Energie Atomique et aux Energies Alternatives (CEA) in France. This irradiation sought to develop and demonstrate the technologies needed to transmute long-lived transuranic actinide isotopes of Pu, Am and Np contained in spent nuclear fuel via fast reactor technology. Postirradiation examination (PIE) of irradiated fuels experiments provides data related to in reactor fuel performance and input into future fuel design choices [2]. The compositions of the FUTURIX-FTA pins were designed to test if minor actinides could be incorporated into the metallic fuel or nitride fuel of a fast reactor without significantly changing fuel performance observed for previously well studied fuels like U-10Zr and U-19Pu-10Zr (where the leading number is weight percent). The fuel performance of metallic fuel in fast reactors has been well documented [3–7]. Other programs and experiments around the world are seeking to demonstrate the safe performance of such advanced fuel both in metallic fuel and other fuel forms [8–11].

This work reports the baseline PIE data for the FUTURIX-FTA metallic fuel pins and discuss these results in comparison with Experimental Breeder Reactor II (EBR-II) and Advanced

Fuels Campaign (AFC) literature. Baseline PIE includes neutron radiography, position sensitive gamma spectrometry, dimensional examinations, fission gas release, optical microscopy, and chemical analysis. These examinations address fuel swelling, fission product distribution, cladding strain, fission gas release, fuel microstructure changes, fuel cladding chemical interaction and minor actinide transmutation. Two metallic alloys were irradiated in FUTURIX-FTA a low-fertile alloy designated FUTURIX-FTA DOE1 and a non-fertile alloy designated FUTURIX-FTA DOE2. Likewise two nitride compounds were irradiated a low fertile nitride FUTURIX-FTA DOE3 and a non-fertile nitride FUTURIX-FTA DOE4. The compositions of these irradiations, the fuel type, and some basic predicted irradiation conditions are given in Table 1. The PIE of the nitride fuels are reported elsewhere [12].

2. Materials

The FUTURIX-FTA metallic fuels were fabricated at Idaho National Laboratory (INL). Short experimental fuel pins (rodlets) were assembled and welded at INL and shipped to CEA in 2006 where extensions were welded onto the short pins to make them the same length as standard Phénix fuel pins.

Table 1. Composition of the FUTURIX-FTA pins

Name	**Fuel Type**	**Composition** *	**Predicted Burnup (%FIMA)**	**Predicted Fission Density (fissions/cm^3)**
DOE1	Metallic low fertile	34.1U-28.3Pu-3.8Am-2.1Np-31.7Zr [U-29Pu-4Am-2Np-30Zr]	9.1	1.99×10^{21}
DOE2	Metallic non-fertile	47.6Pu-10.5Am-0.3Np-41.6Zr [Pu-12Am-40Zr]	15.5	2.46×10^{21}
DOE3	Nitride low fertile	$(U_{0.51}Pu_{0.27}Am_{0.14}Np_{0.08})N$ $[(U_{0.50}Pu_{0.25}Am_{0.15}Np_{0.10})N]$	1.6	4.95×10^{20}
DOE4	Nitride non-fertile	$(Pu_{0.85}Am_{0.15})N+46.5ZrN$ $[(Pu_{0.50}Am_{0.50})N+36ZrN]$	4.1	4.78×10^{20}

*Numbers preceding elements denote weight percent, subscript numbers represent mole percent. This is the as-fabricated composition followed by the nominal composition in brackets

The metallic fuel slugs were prepared using an arc-casting method where the individual feedstock materials are melted together and homogenized into a "button." The button was melted, an uncoated quartz tube mold was dipped into the liquid, and the liquid was drawn up into the mold via suction using a syringe [13]. An example of the final metallic fuel slugs is shown in Figure 1.

The composition and isotopics of the fuel alloys was determined by mass spectrometry. Samples from representative casts of the fuel alloy compositions were characterized for phase formation by X-ray diffraction (XRD), microstructure by scanning electron microscopy (SEM), heat capacities and thermal phase transitions by Differential Scanning Calorimetry (DSC) and Differential Thermal Analysis (DTA) measurements, thermal expansion from Thermomechanical Analysis (TMA) measurements, thermal diffusivity by the laser flash method [13]. Furthermore, fuel alloy resistance to fuel-cladding-chemical-interaction (FCCI) with the AIM1 stainless steel cladding material was tested with a series of diffusion couples [13].

Figure 1. Fuel column of the 34.1U-28.3Pu-3.8Am-2.1Np-31.7Zr composition prior to DOE1 fuel pin loading.

3. Irradiation experiment

FUTURIX-FTA fuel pin is a 352 mm miniature fast reactor fuel rod (rodlet) with ~100 mm fuel column and extensions welded to the top and bottom of each rodlet to allow the fuel to be irradiated using standard, full-length Phénix hardware. Sodium was included in the fuel-cladding gap to improve heat transport between the fuel and the cladding and improve the fuel thermal behavior. The fuel pin cladding is AIM1 [14,15], an austenitic stainless steel provided by CEA as the standard Phénix cladding. Fuel pin parameters are listed in Table 2 and the fuel pin configuration is shown in Figure 2. The FUTURIX-FTA experimental fuel pins were assembled into two Phénix fuel capsules and placed into adapted assemblies. Each Phénix fuel capsule contained 19 fuel pins, 2 experimental pins and 17 standard Phénix driver fuel pins.

Table 2 FUTURIX-FTA Pin Parameters

Parameter	Value
Cladding	AIM1
Fuel Pin Inner Diameter	5.65 mm
Fuel Pin Outer Diameter	6.55 mm
Fuel Column Length	100 mm (nominal)
Short Fuel Pin Length	352 mm
Full Fuel Pin Length	1793 mm

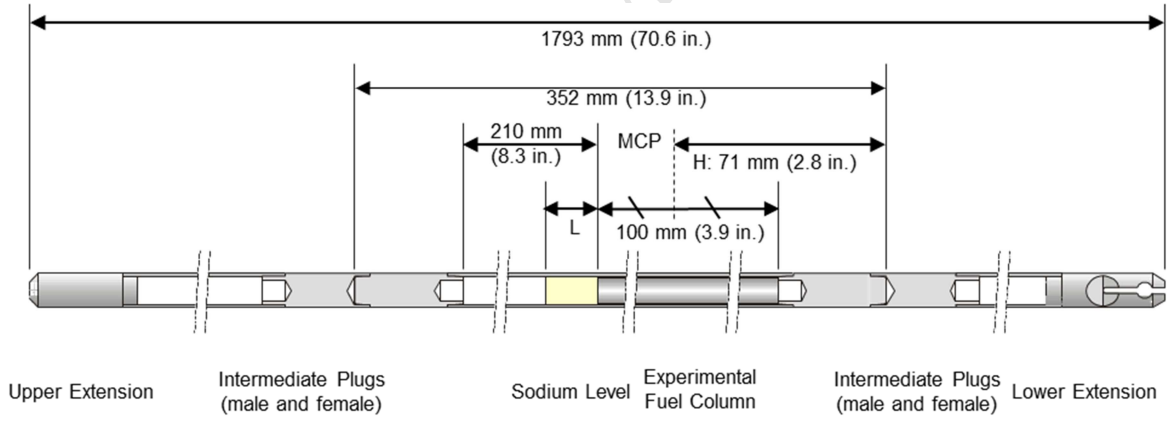

Figure 2. FUTURIX-FTA pin configuration and general dimensions

The metallic fuel pins, DOE1 and DOE2, began irradiation in May 2007 and completed irradiation in May 2009 for a total of 235 EFPD reaching a predicted burnup of 9.1 % FIMA (fission per initial heavy metal atom) and 15.5 %FIMA, respectively (Table 1 reports the predicted burnup and fission density). No sign of fuel pin failure (i.e., loss of tightness) was detected during irradiation.

The linear power heat rate history for the 2 metallic fuel pins is reported in Figure 3, while in Figure 4 the cladding temperature for beginning and end of irradiation (BOI and EOI) is

reported [16]. The peak inner cladding temperature never exceeded 550 °C in either pin. The temperature of the two pins varies axially primarily due to the two pins not being located at the same axial position in the core. The fueled section of DOE1 was placed at core mid-plane with the rod extensions, while the fuel section of DOE2 was placed 25 cm below core mid-plane with the rod extensions.

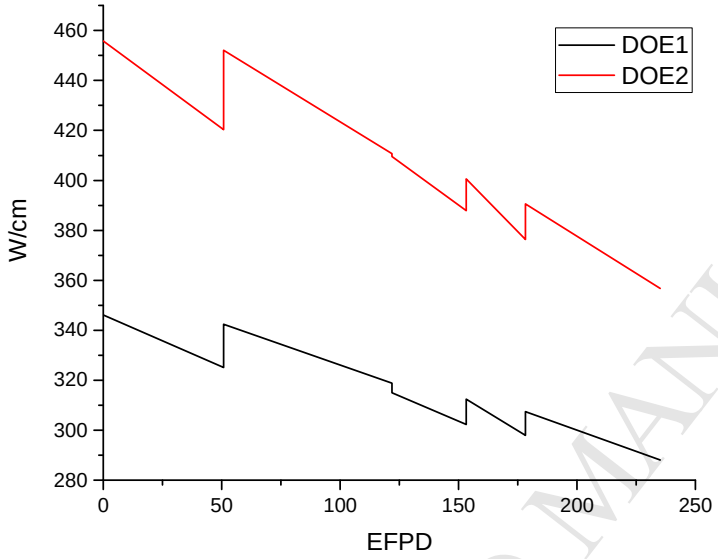

Figure 3. FUTURIX-FTA DOE1 and DOE2 linear power history

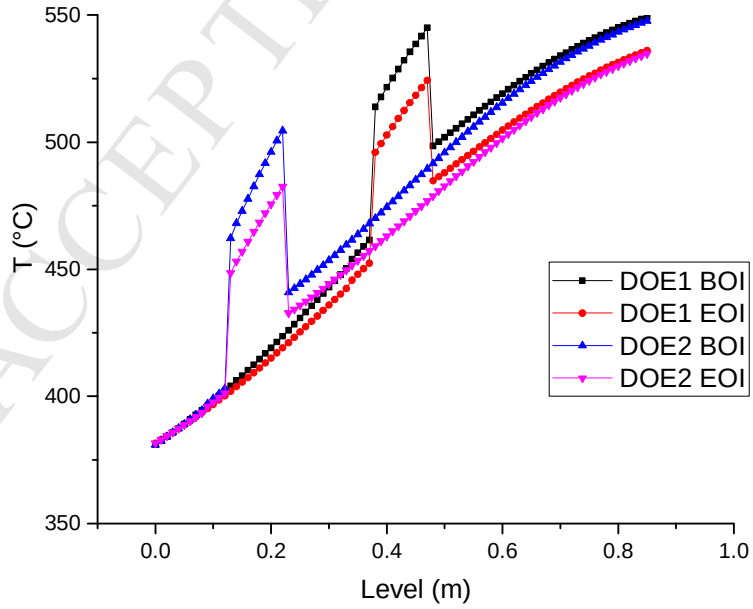

Figure 4. FUTURIX-FTA DOE1-DOE2 inner cladding temperature profile for BOI and EOI

4. PIE results and discussion

Non-destructive examinations of FUTURIX-FTA experiments have been completed at the INL Hot Fuel Examination Facility (HFEF), part of the Material Fuel Complex (MFC). Baseline non-destructive examination includes visual examination by through-window photography, neutron radiography, dimensional inspection, and gamma spectrometry scanning. Furthermore, baseline destructive examinations also incorporates fission gas analysis, metallography observation, and burnup analysis. All these examinations have been completed. Some SEM examinations have also been completed on DOE1 and are also reported in Section 5.

4.1. Axial growth, Geometry retention and Cladding strain

Figure 5 shows neutron radiography of the 2 metallic fuel pins. The radiographs were taken by exposing a Dy foil for thermal neutron radiography and a Cd-covered In foil for epithermal neutron radiography. The exposed foils are then transferred to file and developed [17]. Radiographs were taken at two angles approximately 90° apart. The radiographs from the two angles are similar revealing no major non-axisymmetric features. The fuel has begun to creep down into the void space associated with the bottom endplug (especially visible in the DOE2 pin). This is highlighted in Figure 5a as the area between the two red arrows. This growth is not a significant contributor to axial growth. There is also no evidence of the fuel slug separating from the lower end-plug. This phenomenon was known as “lift-off” and occasionally occurred in EBR-II pins [18,19]. This creep down phenomena was already observed and studied during EBR-II experiments, and it is reported to not cause degradation of fuel performance or life time [20]. The bond sodium above the fuel appears to be free of any dissolved fuel material. It is possible to see some gaps between fuel slugs that generally correspond to the original fuel slug dimensions. This indicates very little axial growth in these fuel slugs, approximately 0.5% for DOE1 and 3% for DOE2. Little comparable data exist for these 2 alloy compositions in literature. Furthermore, there is a lack of consensus among experts concerning how to understand the phenomenon of axial growth in metallic fuels. There is some evidence that suggests axial growth in metallic fuel may be in part an end effect that happens in close proximity to the unconstrained, free fuel surface at the top of the fuel column. For example, measured axial growths in FFTF irradiations of metallic fuel have been noted to be less than those for identical compositions in EBR-II [21]. Compared to

the literature for U-(0-26)Pu-10Zr [7], DOE1 had very little growth which perhaps stems from the higher content of Pu and Zr, while DOE2 is in line with axial growth at 15 %FIMA burnup of a U-19Pu-10Zr [7,22].

There is some enhanced neutron attenuation in the epithermal image in the central region of DOE2 (Pu-10.5Am-41.6Zr) above what is expected from the curvature of the pin. This could indicate either a change in bulk density in the central region of the pin or a change in composition that has enhanced resonance neutron absorption in the central region of the pin. Plutonium and americium isotopes have a number of large resonances above the Cd cut-off energy that could contribute to the features seen in Figure 5b. This feature may indicate some constituent redistribution has occurred. In this alloy the redistribution may not follow the same well studied trends seen in U-10Zr and U-19Pu-10Zr [4], and Pu or Am may densify in the center of the fuel. Spatially resolved chemical analysis of this fuel pin with SEM and energy dispersive spectroscopy (EDS) or electron probe micro-analyzer (EPMA) would be necessary to fully understand the observed change in attenuation.

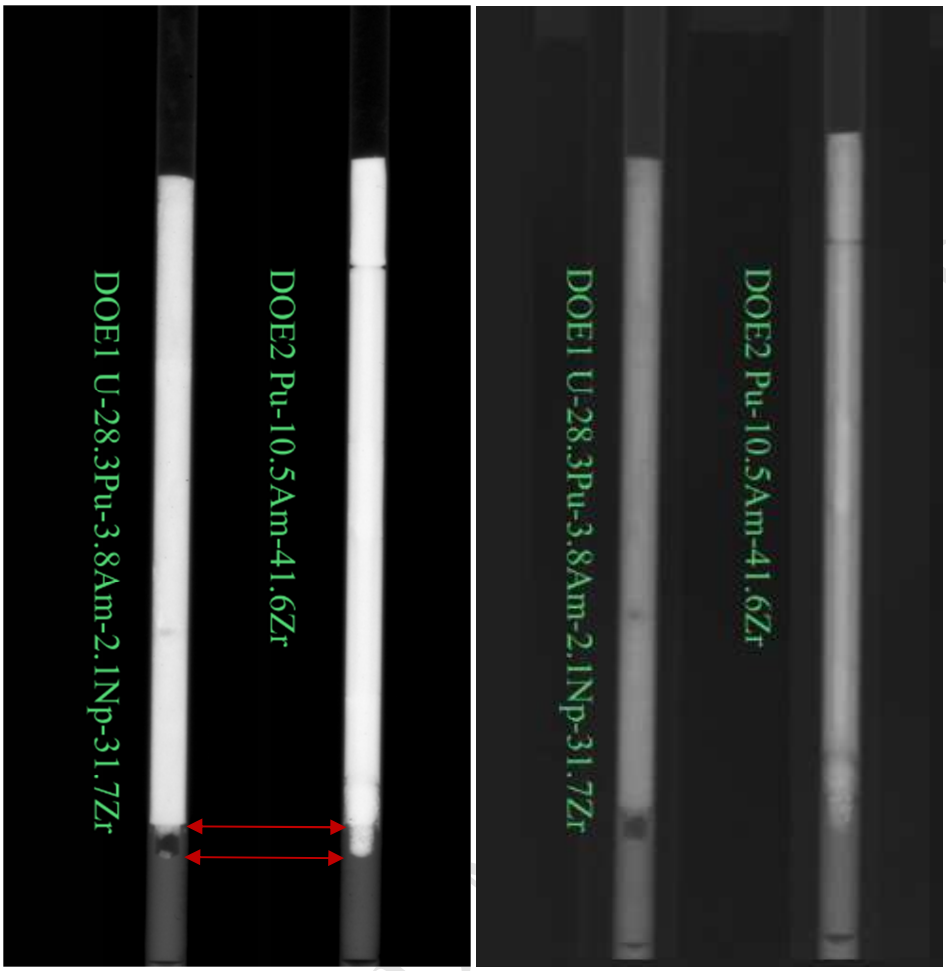

(a) (b)

Figure 5(a). Thermal neutron radiograph (b) Epithermal neutron radiograph of the fueled region of the FUTURIX-FTA metallic alloy pins.

Cladding diametral strain was measured by the HFEF element contact profilometer. Diameter measurements were collected all along the pins in roughly 0.127 cm increments and at 6 angles spaced 30° apart. Diameter measurements are collected with ±5 µm accuracy.

Figure 6 reports the measured diametral strain for DOE1 (Figure 6a) and DOE2 (Figure 6b). The off-scale jumps in strain indicate the locations of welds where the rodlets are attached to endcaps and extensions. The rodlets are shown plenum to the right and fuel zone to the left. The fuel zone starts 1.5 cm from the bottom of the rodlet endcap. The uncertainty shown for each measurement is 7.7×10^{-4}, which is the 1 sigma uncertainty.

Thus while there is a consistent strain indicated in the fuel zone of DOE1 and DOE2, this strain is at the limit of the sensitivity of the instrument which cannot quantify strain below 0.1%. The slightly larger peak seen at about 9 cm for DOE2 in the 30° scan is likely surface

contamination since this deformation is not seen in the other scans. In the METAPHIX experiment [9] and EBR-II fuel pin with D9 cladding [7] higher diametral strain is reported. This might be an indication that higher Zr content and the absence of U in DOE2 limits the anisotropic and elevated swelling behavior of alpha-U.

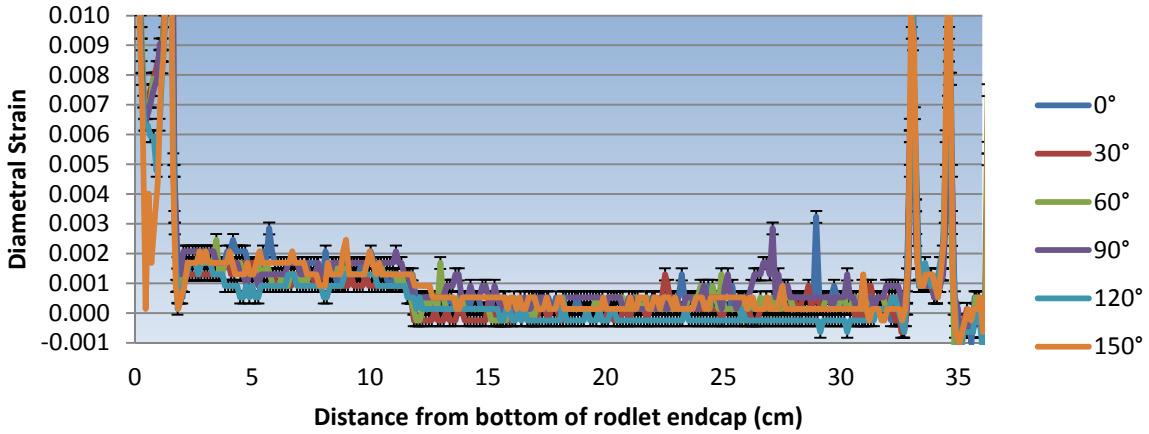

(a)

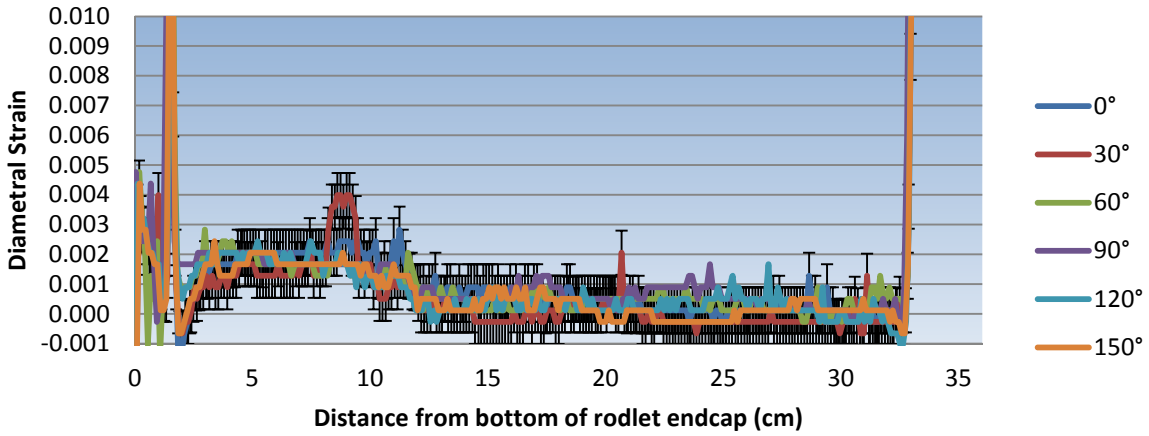

(b)

Figure 6. Diametral cladding strain measured for DOE1 (a) and DOE2 (b).

4.2 Solid and Semi-volatile Fission product behavior (Gamma spectrometry & Tomography)

Gamma spectrometry was performed on both pins. The plenum portion of the pin was scanned in 0.254 cm steps, and the fuel section of each pin was scanned in 0.127 cm steps for a live time of 30 minutes. Axially distributed gamma spectrometry results from selected

isotopes for the low fertile metallic fuel alloy DOE1 and non-fertile metallic fuel DOE2 are shown in Figure 7 and Figure 8 respectively. The distribution of the selected isotopes is discussed below. The thermal neutron radiography for the specified pin is also shown in these figures to help illustrate the location of the fuel and endcaps in relation to the gamma spectrometry data.

In the HFEF Precision Gamma Scanner (PGS) [23], fuel pins are typically suspended vertically using a stage that has horizontal, vertical and rotational motion. Typically fuel pins are scanned in the vertical direction with the collimator in the horizontal position. The collimator is rectangular with a 2.22 cm width and a height that can be varied from 0.0254 cm to 0.254 cm. In addition to the typical axial gamma spectrometry scans, it is possible to rotate the HFEF PGS collimator from a horizontal to a vertical orientation. In this orientation it is possible to move an axial level of the fuel past the collimator and perform a series of rotations over several angles. The resulting signals over several angles can be collected and tomographically reconstructed to provide a two dimensional distribution of fission products averaged over an axial location. This technique is referred to as Gamma Emission Computed Tomography (GECT). The full details of this technique are available in [24], and other demonstrations of this technique can be seen in References [25,26].

The GECT technique was applied to both DOE1 and DOE2 in 0.0254 cm steps over 16 equally spaced angles between 0 and 180°. For both pins, data was collected at the mid-plane of the fuel slug.

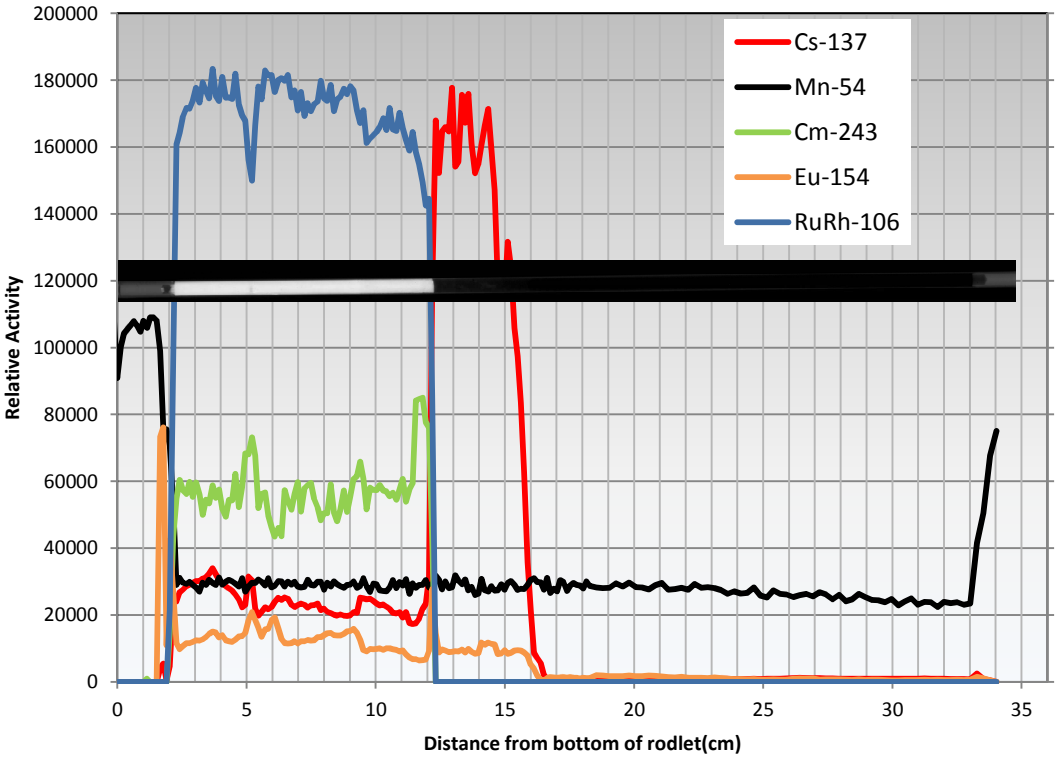

Figure 7. Axial distribution of select gamma emitting radionuclides in FUTURIX-FTA DOE1 (low fertile metallic).

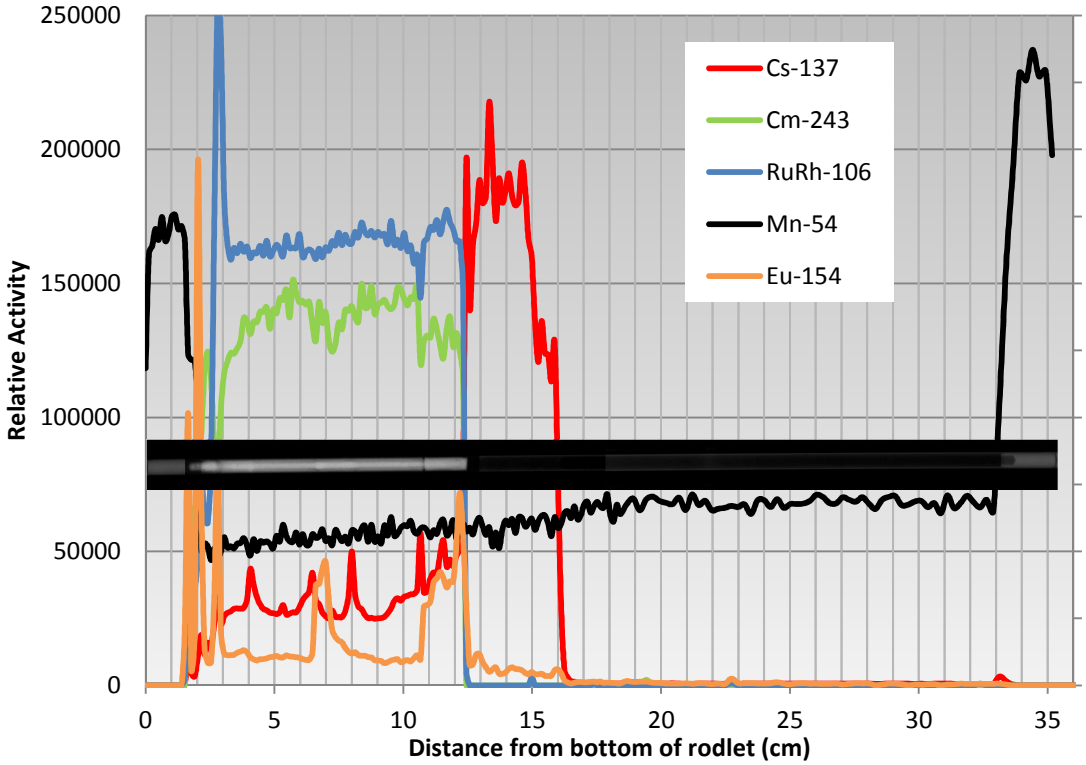

Figure 8. Axial distribution of select gamma emitting radionuclides in FUTURIX-FTA DOE2 (non-fertile metallic).

Cesium

In metallic fuel, Cs isotopes produced by fission are often dissolved in the Na bond between the fuel and the cladding. The Cs migrates with the Na above the fuel column producing a Cs activity spike above the fuel. There are also Cs spikes present at the interface between different slugs used to create the DOE2 fuel stack. This is highlighted in Figure 8 with image overlays of the neutron radiography where gaps align with the Cs signal spikes at 4, 8 and 10.5 cm above the the bottom of the rodlet.

The tomographic distribution of Cs-137 is notable and different for the two pins as shown in Figure 9. In DOE1 (Figure 9(a)), Cs-137 is present across the radius of the fuel and spikes to a high concentration at the center of the fuel. This distribution may be indicative of a great deal of open porosity in the interior of the fuel pin at this level (this is confirmed by optical microscopy in Section 4.4 of this manuscript). Therefore Cs-Na has infiltrated the porosity in this region. In the past, a similar Cs spike was also observed in the fuel interior. During the Integral Fast Reactor (IFR) program a punch electrical discharge machine (EDM) was used to look at several radial positions in irradiated U-20Pu-10Zr metallic fuel. When the samples were counted the Cs profile matched the distribution seen in Figure 9(a). However, at the time this result was viewed with skepticism and was not published [27]. Further investigation into this aspect might be warranted, as this behavior could have implications on how the thermal behavior of the fuel is modeled, and it may be possible to infer the extent of Na logging present in a pin by this method. The observed Cs distribution in DOE2 (Figure 9(b)) is quite different. It appears to be concentrated in a ring around the fuel slug as is typically observed in other metallic fuel [6,7].

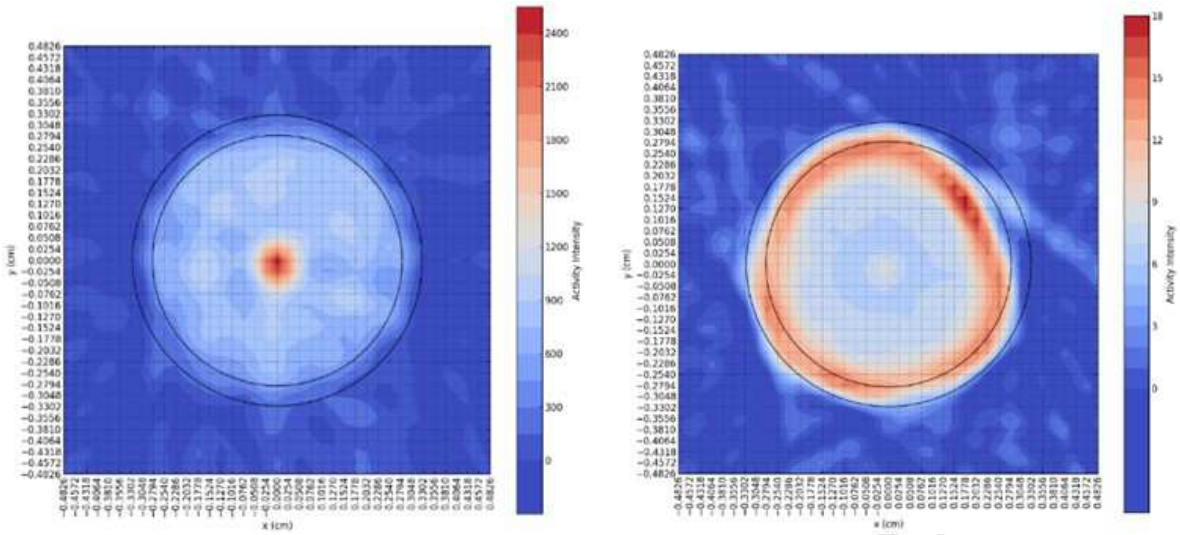

a) b)

Figure 9. Cs 137 Distribution in the middle of the fuel zone for DOE1 (low-fertile metallic) (a) and DOE2 (non-fertile metallic) (b).

Noble metals: Ruthenium / Rhodium

The noble metals Ru and Rh are assumed to be fully miscible in the fuel structure, and the signal strength is a good measure of fuel density at a given axial location. Often Ru-103 can be seen in PIE gamma spectrometry, but the time elapsed from end of irradiation to PIE was too great for FUTURIX-FTA. The location of Ru-106 is inferred from its short lived daughter isotope Rh-106 hence the signal is often referred to as RuRh-106. The dip in RuRh-106 signal at 5 cm in Figure 7 coincides with a void seen in the neutron radiography at this height. There is a similar dip in Figure 8 at 10.5 cm that corresponds to a gap that has formed between the two fuel slugs. Also, the spike in RuRh-106 signal at the bottom of the fuel stack in Figure 8 appears to be due to a sharp drop in the local density of the fuel that reduces the attenuation of the gamma-rays. This spike corresponds to the creep of fuel down into the endplug volume seen in the neutron radiography (see Figure 5).

The tomographic distribution of Ru-106 for both DOE1 and DOE2 are similar and shown in Figure 10 and it appears to be a ring at the periphery of the swollen fuel slug. The reduced level of Ru-106, and by implication lower fission rate, in the center of the rodlet may have resulted from a significant Zr redistribution into the fuel center which is likely for DOE1 and DOE2 based on observed Zr redistribution behavior in metallic fuels from EBR-II [4]. Additionally for DOE1, the ring distribution of Ru-106 may also be indicative of the open

porosity forming in DOE1 that was indicated by the Cs signal. The ring of Ru may also be an indication of Ru mobility above a certain temperature where the Ru is moving out of the hot central region of the fuel into the cooler periphery of the fuel. This latter possibility was observed in an EPMA study of U-Pu-Zr irradiated in Phenix where Zr-Ru blocky particles are found in a ring in the periphery of the hot central region [9].

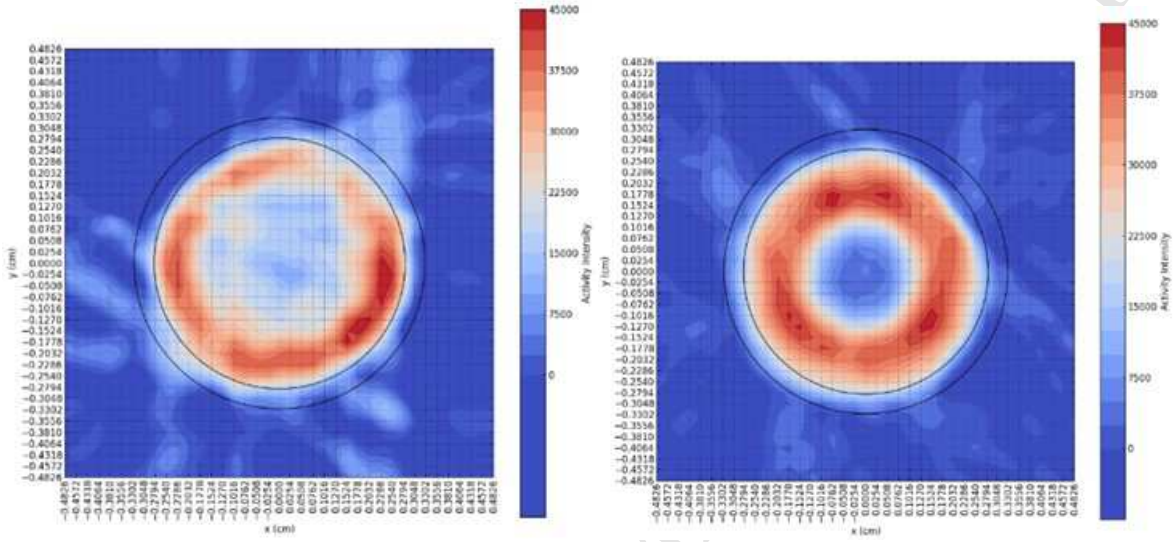

a) b)

Figure 10. Ru-106 Distribution in the middle of the fuel zone for DOE1 (low-fertile metallic) (a) and DOE2 (non-fertile metallic) (b).

Lanthanides: Cerium / Praseodymium and Europium

The axial distribution of CePr-144 was not plotted in Figure 7 or Figure 8. The axial distribution was relatively flat. There is no evidence of significant rare earth (Ce) migration to the fuel periphery which might indicate unexpectedly high levels of fuel cladding chemical interaction as reported in literature from Porter and Tsai [21]. The relative level of Ce migration to the fuel periphery is measured by comparing the Ce-144 activity calculated by the 133.5 keV gamma-ray and the higher energy (696, 1489 and 2186 keV) gamma-rays from the daughter of Ce-144, Pr-144, that is in secular equilibrium with Ce-144.

While europium is classified broadly as a lanthanide, it exhibits different behavior than the lighter lanthanides (La, Ce, Nd). The axial distribution of Eu-154 indicates Eu has migrated at the 2 extremities, top and bottom of fuel as shown in Figure 7 and Figure 8. This behavior has been observed also in other experiments [26,28] and is reported here for these alloys .

Curium

A strong gamma-ray signal was also detected from Cm-243 which is likely due to the significant Am content in the fuel initially. It is not clear with the present PIE data if this signal can be used to infer the position of Am in the fuel or if its distribution is more indicative of independent Cm chemistry. The Cm-243 axial distribution in DOE1 is fairly flat with the exception of a spike at 5cm and between 11 and 12 cm in Figure 7. The 5 cm spike may indicate Am migrating into the 5 cm void identified early in the discussion on RuRh-106 signal. The upper fuel column spike may indicate migration of Cm or Am towards the fuel periphery at this height. The most notable feature in the Cm-243 signal in Figure 8 is the signal shift at 10.5 cm where two fuel slugs meet. The shift in signal intensity between the two slugs may indicate non-uniform Am loading between the two slugs.

The Cm-243 tomography redistribution is shown in Figure 11, and this result is also difficult to interpret. The signal strength from DOE1 is not excellent, but generally appears to be a fairly constant distribution across the fuel. Local variations in Figure 11are likely due to statistical variations in the collected spectra. The signal from DOE2 indicates a ring where no Cm 243 is located. This may suggest some chemical migration in the fuel that has shifted the Am or Cm concentration away from the mid radius of the fuel.

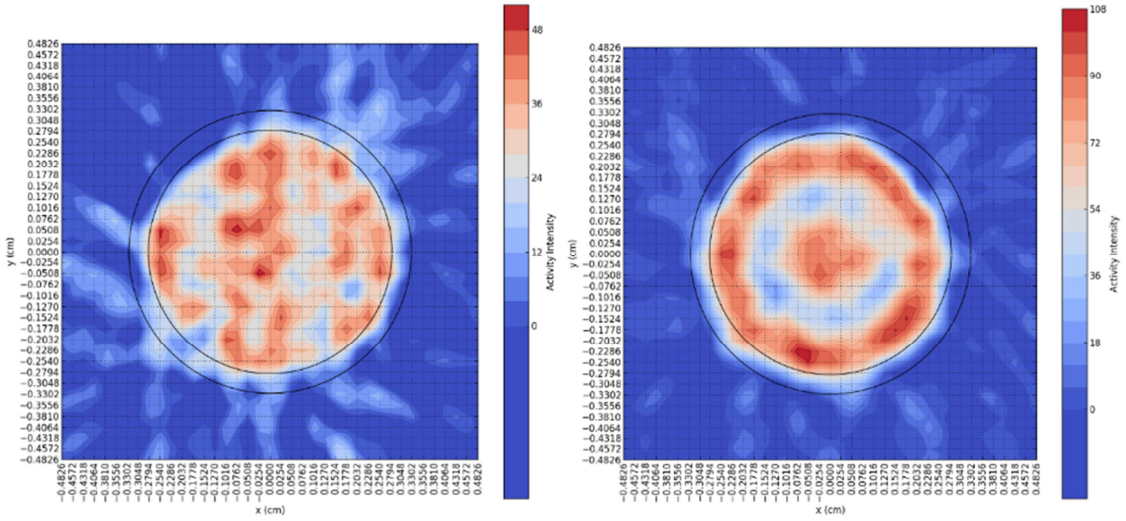

a) b)

Figure 11. Cm-243 Distribution in the middle of the fuel zone for DOE1 (a) and DOE2 (b)

4.3 Fission product gas behavior

Fission gases were collected from the pins using the HFEF Gas Assay, Sample, and Recharge (GASR) system. Pins were punctured using a 150 W Nd-YAG laser system, and a gas sample was collected in a stainless steel bottle external to the hot cell. Void volume in the pin was then determined by a series of backfills into the punctured pin and expansions into the GASR system. The pin internal gas pressure was derived from the void volume measurement and the initial gas pressure measurement upon puncture. Ideal gas behavior was assumed in determining internal gas pressure. Fission gas analysis was performed by gas mass spectrometry. Results of fission gas analysis provided total elemental composition including He, krypton isotopic composition, and xenon isotopic composition. A summary of results is shown in Table 3. The combined Kr and Xe release is the ratio of the number of fission gas atoms (Kr+Xe) measured in the plenum to the number of fission gas atoms produced by fission. The number of fissions in each rodlet was determined from ICP-MS discussed in Section 4.5, and the number of fission gas atoms produced per fission is estimated from the fast fission yields for Kr and Xe found in ENDF/B-VII.1[29].

The FUTURIX-FTA pins were welded in a 75% Ar, 25% He gas mixture. The total number of moles of gas present in the plenum can be calculated from the plenum pressure and the plenum volume using the ideal gas law. The PIE amount of Ar was compared to the expected amount of Ar in the pin from fabrication, and the two values were found to agree within less than 4%, indicating good samples were collected by GASR without any contamination from the argon atmosphere in the HFEF hot cell. The resulting fission gas releases are reasonable. The metallic fuel fission gas release is close to the 70%±10% release that is expected from typical 75% smeared density U-Pu-Zr fuel behavior beyond 5 at.% burnup (or 1×10^{21} fissions per cm^3) after porosity interconnects [6,7]. The release value for DOE1 is a little low compared to literature, but still comparable to the historical band data from EBR-II, as shown in Figure 12. The DOE2 fission gas release is exactly in line with historic expectations of metal fuels. There are some anomalously low fission gas release values from the EBR-II data at higher fission densities (4.5-6.0 fissions/cm^3). These values are reported here for completeness, but they are likely erroneous data generated by a poor puncture. In general, the fission gas release values from the FUTURIX-FTA metallic fuels are also in reasonably good agreement with values from the AFC-1 experiments irradiated in ATR [30–32], as can also be observed in Figure 12.

The helium release was 62 and 64% for these 2 pins. This release is primarily from the α decay of the minor actinides present in this fuel and must be considered in high burnup minor actinide bearing fuel pins due to its impact on plenum pressure. This release is low when compared to literature values: METAPHIX reported a release around 100% [8] and EBR-II X501 experiment reported a release of 90% at burnup of 7.6 %FIMA [33]. However, there is not a large historical data base for He release from minor actinide bearing fuels and the uncertainty on such measurement is quite high.

Table 3. Fission Gas Release Summary

Fuel pin	Kr+Xe Gas Release (%)	He Gas Release (%)
DOE1	51.6%	62.4%
DOE2	69.3%	64.2%

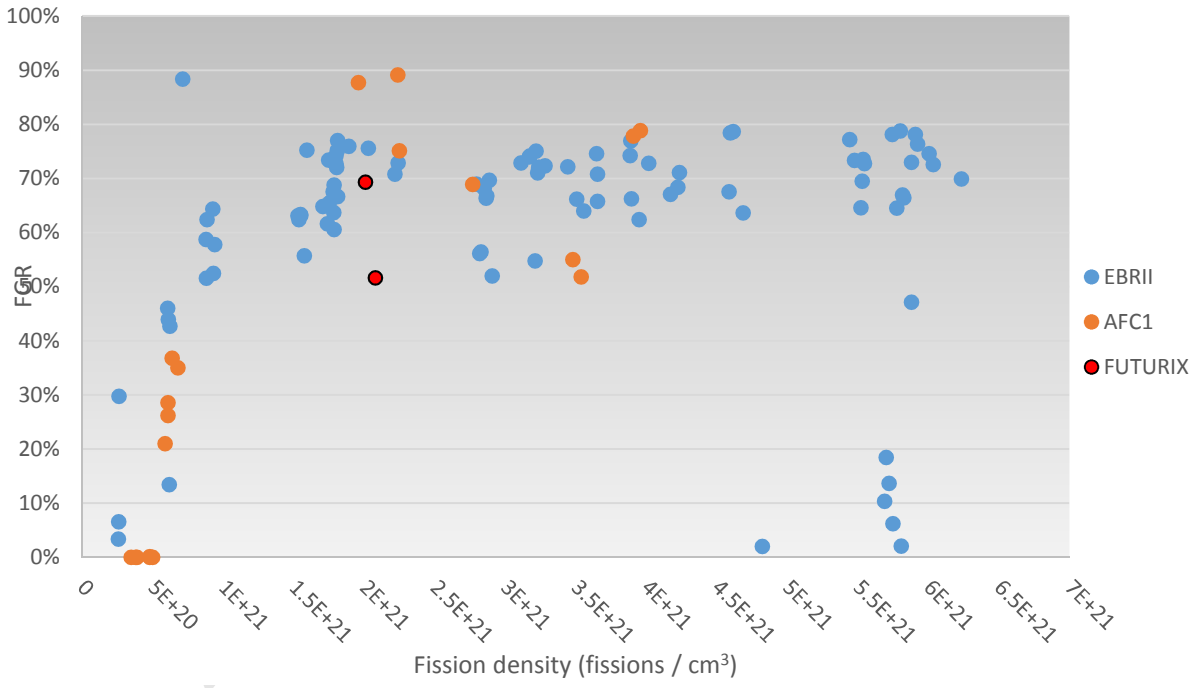

Figure 12. Fission gas release versus fission density for AFC-1 [30,31], FUTURIX-FTA (metallic alloys), and the historic EBR-II database ***[3,5,6]***

4.4 Fuel microstructure and restructuring

Fuel microstructure was investigated using optical microscopy, also referred to as metallography. Pins were sectioned through the fuel zone in order to create samples for

optical microscopy. Cross-sections about 6 mm in length were cut, mounted in epoxy, and polished to a 0.25 µm finish. Optical microscopy was performed on a Leitz MM5RT metallograph installed in a shielded inert atmosphere alpha containment hot cell. Radial cross-sections were taken from the midplane or slightly below midplane of the fuel column; samples were not taken near the ends in order to avoid possible peaking or end effects.

DOE1 (U-28.3Pu-3.8Am-2.1Np-31.7Zr)

The cross section of DOE1 is revealed in Figure 13 and in greater detail in Figure 14. The microstructure reveals a porosity that is spherical in shape throughout most of the fuel, apart from the very outer periphery of the fuel where it is smaller and somewhat lenticular. The circular porosity region stretches from the center of the fuel out to a radius of about 2.3 mm. This would tend to indicate that the underlying crystal structure of the fuel material is cubic similar to γ-(U,Zr) [3,4,7] everywhere except the outer 500 µm.

The peak cladding temperature of DOE1 was predicted to be approximately 550°C (as can be seen in Figure 4), and from Reference [34] it can be observed that alloys of U,Pu,Zr have a phase transitions into BCC phase (that is akin to γ-U) that occurs at temperature lower than 650°C when Pu and Zr contents are ~30 wt.%. This thermophysical behavior would explain the spherical porosity wide spread to most of the fuel sample and the presence of periphery region of the fuel showing non-spherical porosity where the irradiation temperature was below the γ-U phase transition temperature. Additionally, with the amount of central porosity seen in Figure 13 and Figure 14, the Cs behavior seen in Figure 9 appears more reasonable. The Cs distribution indicates that Cs has likely dissolved into the sodium, and the sodium has likely infiltrated into the highly porous structures seen in the micrographs.

This microstructure characteristic can be directly compared with the EBR-II X501 transmutation experiment [33] in which a minor actinide bearing metallic fuel alloy U-20.2Pu-9.1Zr-1.2Am-1.3Np was irradiated to similar irradiation conditions of 7.6 %FIMA burnup with a calculated peak cladding temperature of 540°C. Figure 15 reports an optical cross section image of X501 fuel. The central region (~1.2 mm diameter) is much smaller in the X501 fuel compared to DOE1 (Figure 13). This is expected since the Pu and Zr content of this fuel is lower than in DOE1. This metallic alloy (~U-20.2Pu-10Zr) has a phase transition

temperature to the cubic high temperature phase (γ-U) around 650°C [7,34] higher than what is expected for the DOE1 cubic phase transition.

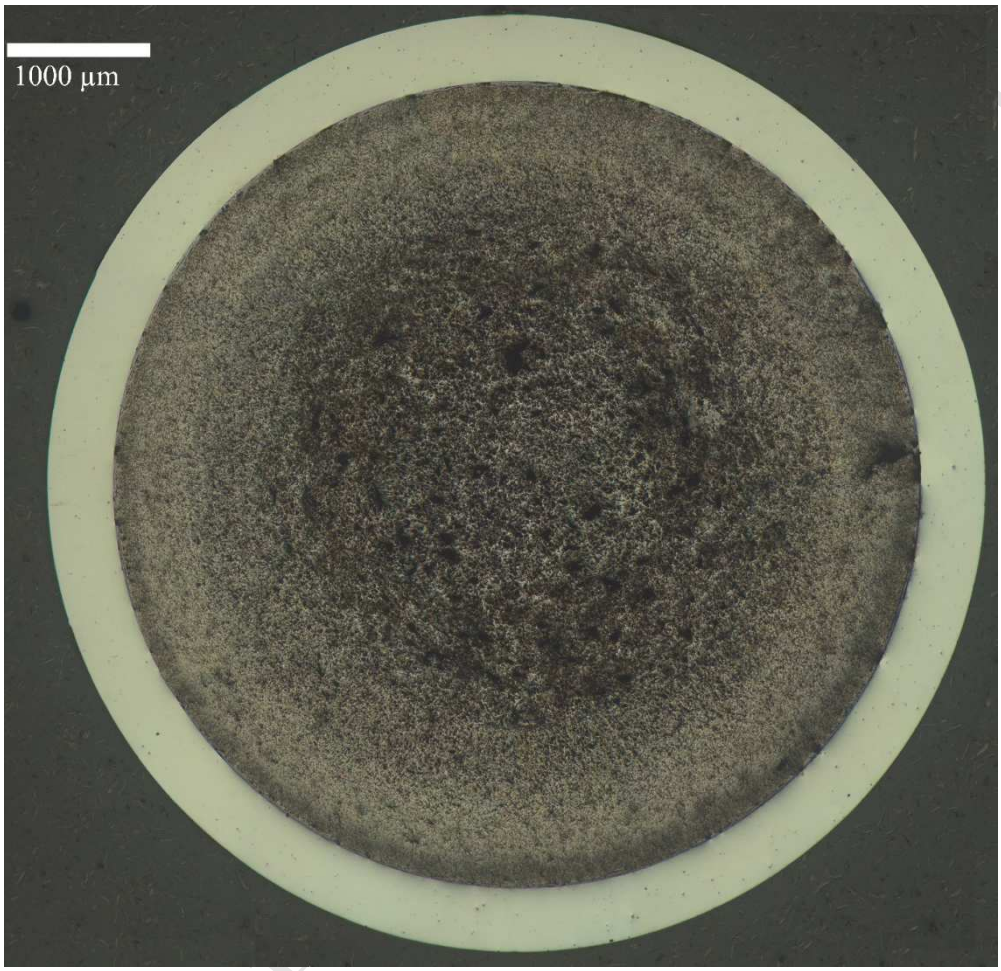

Figure 13. Montage of images of cross section of DOE1 (low-fertile metallic).

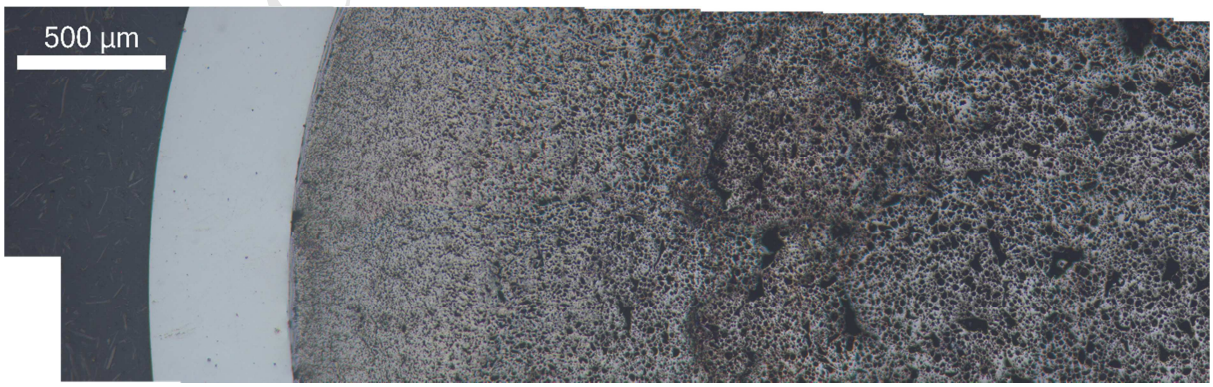

Figure 14. Higher magnification detail of radial microstructure of DOE1 (low-fertile metallic).

Figure 15. X501-G582 cross section optical image (taken from [33])

Figure 16 details a small (~20µm) interaction layer at many locations between the fuel and the cladding. Optically this cannot be positively identified. This may be the initiation of a FCCI layer, or it may be an artefact of fabrication. There was also a Zr rich layer at the edge of the as-fabricated samples [13]. Furthermore, Figure 17 shows the detail of observed secondary phases in the fuel inferred to be precipitates of rare earths with Am/Cm based on prior irradiations of metallic fuel [35] and metallic fuel with minor actinides [33].

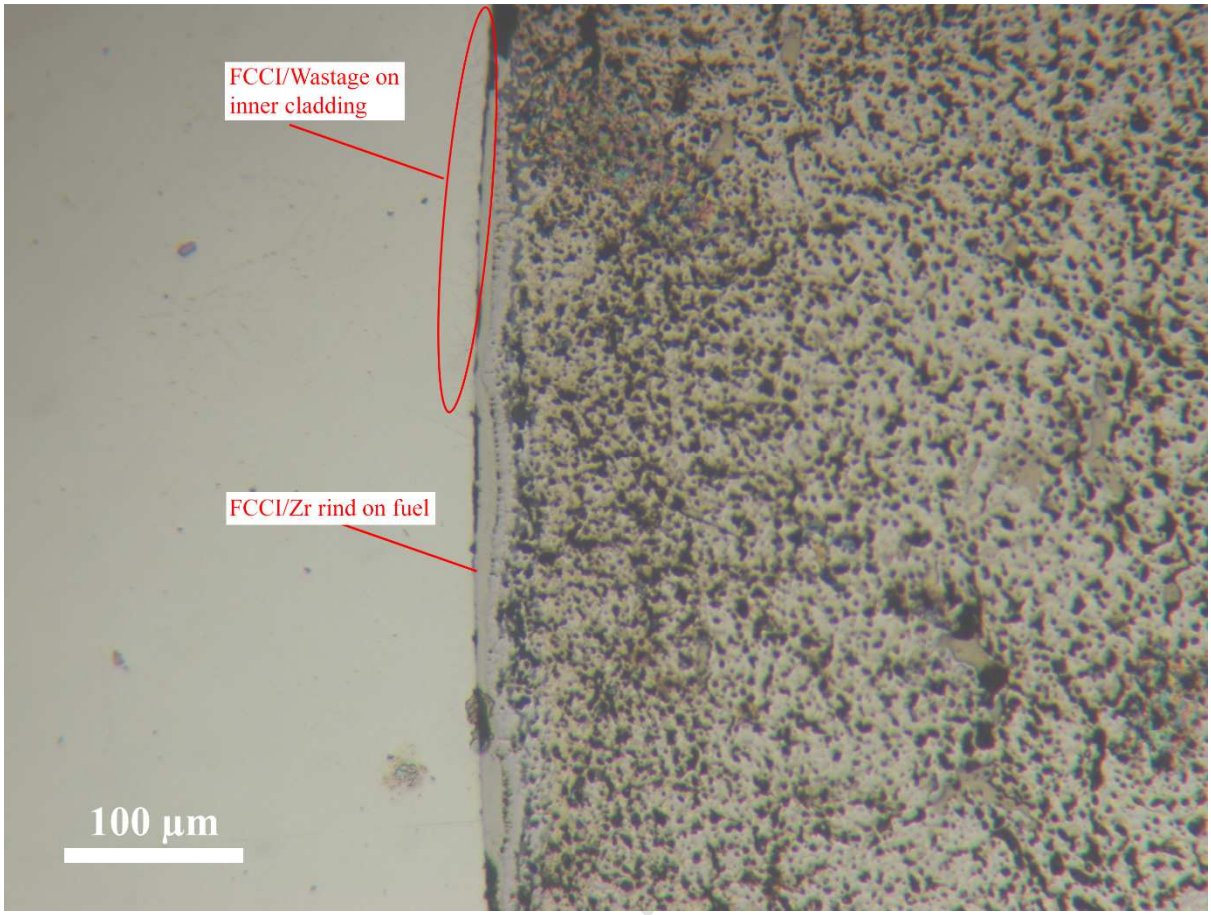

Figure 16. Higher magnification detail of the FCCI region from Figure 14

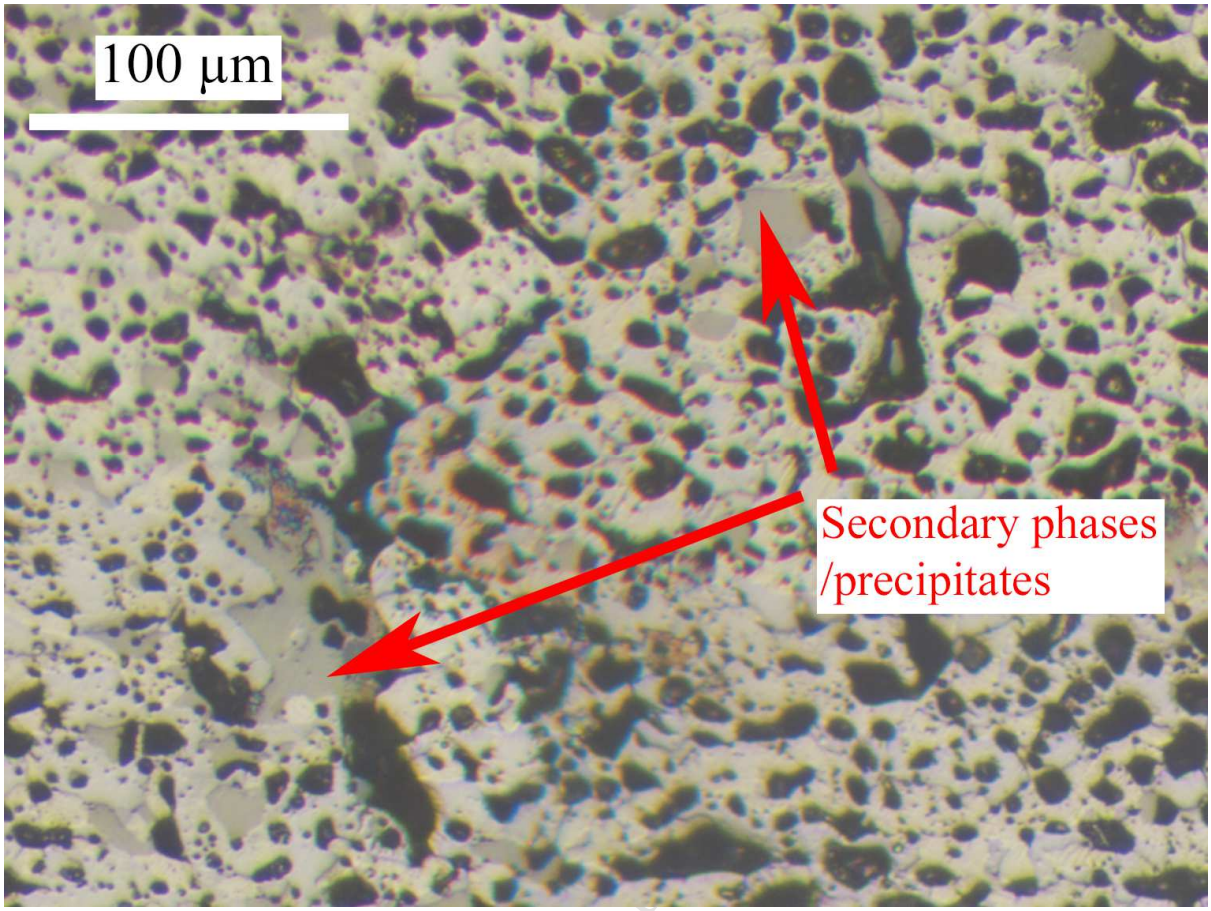

Figure 17. Higher magnification detail of secondary phases precipitates in DOE1

DOE2 (Pu-10.5Am-0.3Np-41.6Zr)

The cross section from DOE2 is shown in increasing detail in Figure 18, Figure 19, and Figure 20. The cladding has several spots with debris and tarnishing from polishing. The black marks on the cladding in Figure 18 should not be mistaken for cladding degradation. This cross section shows evidence of constituent redistribution and phase separation. There are several rings of microstructure present in Figure 19 that suggest different phases that were present during irradiation and these phases are likely driven by different thermal conditions present in the fuel during irradiation. The Pu-Am-Zr system is not as well understood as the U-Zr or the U-Pu-Zr system, but many of the same observations made on the DOE1 cross section can be made and tied back to known properties of the Pu-Zr system. As-fabricated, XRD of the fuel revealed the predominant microstructure to be δ-(Pu,Zr) [13]. During irradiation the peak cladding temperature was about 550°C, so it is likely that during irradiation both δ-(Pu,Zr) and ε-(Pu,Zr) were present in the fuel. Both of these phases are cubic and the porosity structure suggests a cubic crystal structure. As in DOE1 there is a ~20µm layer that is likely a Zr rich layer from fabrication, or it could be a FCCI interaction

layer. There are 5 major zones of microstructure in the fuel. The first three from the outer radius of the fuel inward about 1 mm all have small porosity and varying amounts of what appears to be phase separation supposed by different colors in the microscopy which often indicates various different levels of oxidation. Certain layers oxidize faster than others presenting a different color. In the next 750 µm, the porosity of the fuel changes significantly and becomes much larger. The color of the fuel matrix also suggests that this is a more homogeneous phase in the fuel. This is all visible in Figure 18 and Figure 19. The interior of the fuel has a great deal of phase separation. In Figure 19, one of phases is much more susceptible to oxidation and is orange in the collected microscopy. The orange phase tends to cluster and is surrounded by a lighter matrix phase. The matrix phase is shown in detail at the center of Figure 20 and has a stacked or lamellar structure. Here this phase is shown 30 µm.wide. It is assumed that the appearance of the stacked or lamellar structure is an indication of a different chemical phase not a different crystallographic orientation in the material. The individual lamellae are on the order of a few µm wide as highlighted in Figure 20. The lamellar structure of the matrix phase is suggestive of the decomposition of γ(U,Zr) into αU and δUZr_2. The stacked structure in this fuel could be the decomposition of ε-(Pu,Zr) into δ-(Pu,Zr) and αZr. If Zr redistribution did drive additional Zr up the temperature gradient to the center of the fuel this explanation is also more likely.

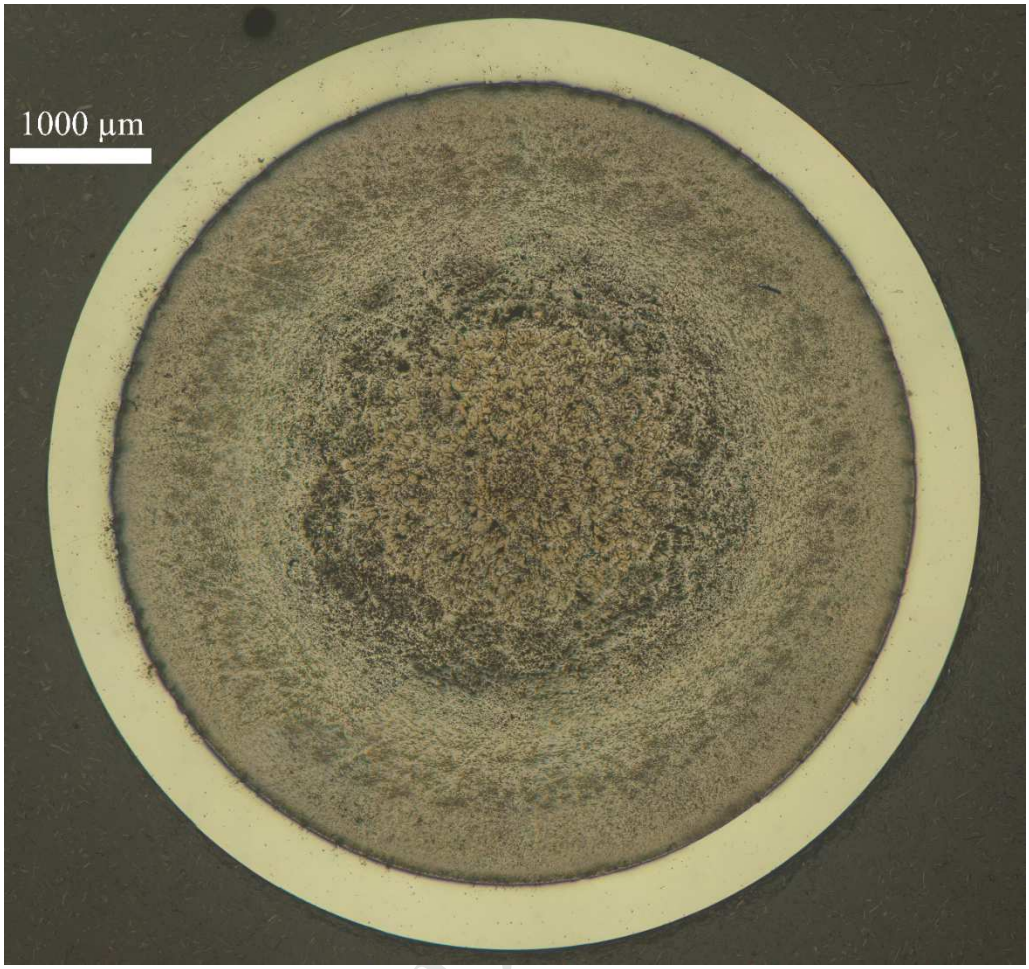

Figure 18. Montage of images collected from cross section of DOE2 (non-fertile metallic)

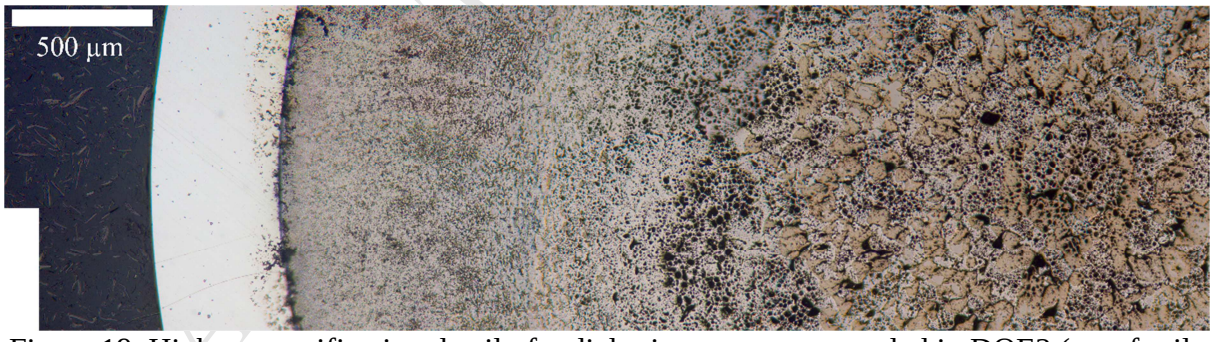

Figure 19. Higher magnification detail of radial microstructure revealed in DOE2 (non-fertile metallic).

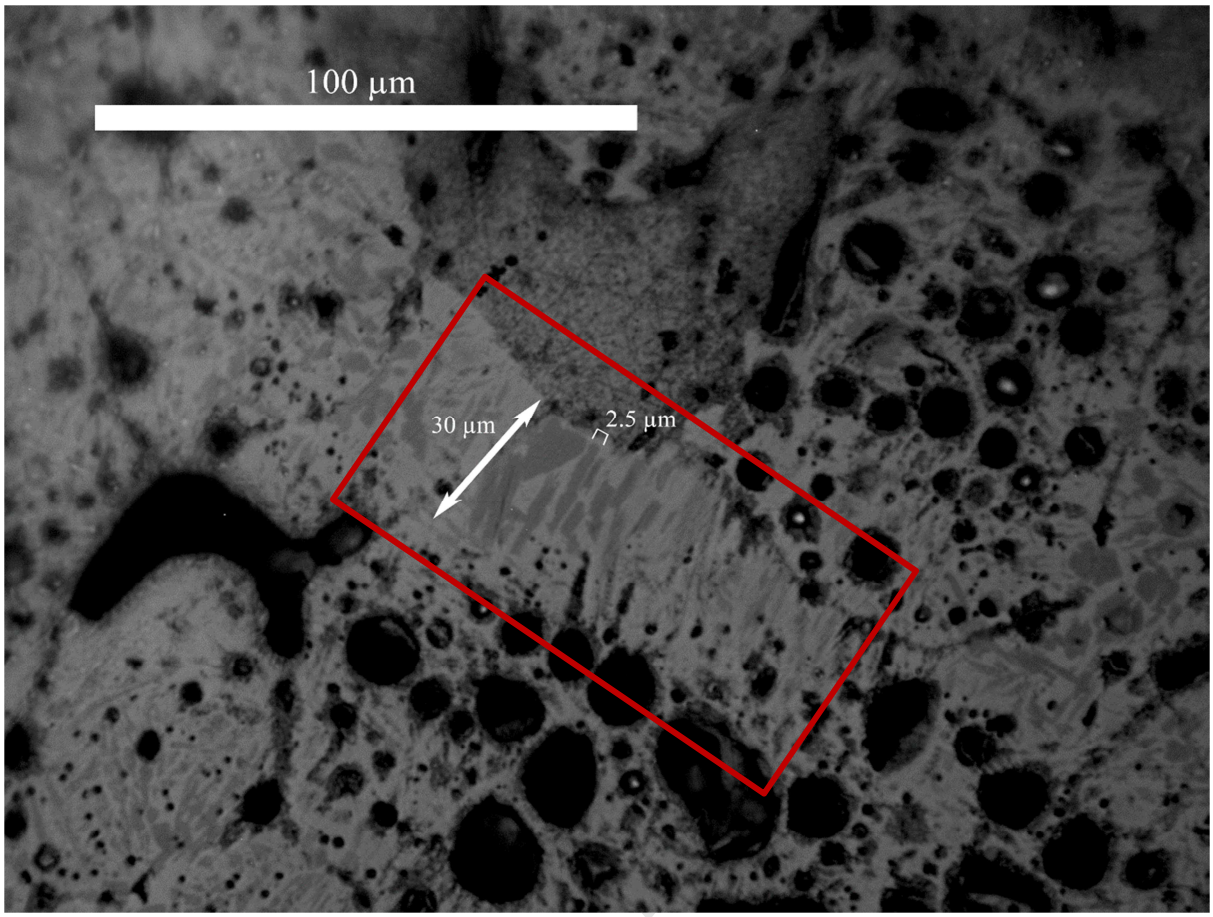

Figure 20. A representative detail of phase separation present in the central region of DOE2. The stacked or lamellar structure of a distinct portion of the matrix phase is stressed by the red rectangle in the center of the figure.

4.5 Burnup measurement

During pin sectioning to create the microscopy samples, additional samples were taken from near the fuel stack center and sent to the INL Analytical Laboratory (AL) for a variety of chemical and radiological analyses. The primary goal of the analysis is to ascertain the burnup of the sampled material. Gamma spectrometry analysis is also performed. Axial variations in burnup along a pin, if any exist, can typically be scaled by comparing quantitative gamma spectrometry results from the AL to semi-quantitative results from PGS.

Burnup is calculated from the results of mass spectrometry examinations of dissolved fuel samples. Samples are placed in a heated acid solution until both the fuel alloy or compound and the cladding have dissolved. Care is taken to ensure complete dissolution of all constituents which can take up to 24 hours to complete. Metallic fuel samples were dissolved in 9M HCl.

Aliquots of the original dissolution are diluted and sent through different inductively coupled plasma mass spectrometry devices (ICP-MS). Samples are sent through an ICP-AES (atomic emission spectrometry) to determine the cladding and sodium weight of the sample. The derived cladding weight is then subtracted from the balance measured as-received sample mass. Samples are removed from the hot-cell and sent through an ICP-MS to determine the isotopic composition of the major constituents and fission products. In many cases there are isobaric (same atomic number) interferences that prevent exact identification of isotopic species. In the fission product data, isobaric interferences were not considered significant to the conclusions of this study, so no additional separations were performed to clear these interferences. The primary isobaric interferences in the actinides are from Pu. To remove the Pu from the solutions, they are passed through an Eichrom TEVA Resin. Pu is retained in the resin and all other actinides pass through. The Pu solution and the mixed actinide (Th, U, Np, Am, Cm) are analyzed by the ICP-MS. The ICP-MS results were able to produce isotope specific results for U-234, U-235, U-236, U-238, Pu-238, Pu-239, Pu-240, Pu-241, Pu-242, Np-237, Am-241, and Cm-244. The combined mass of Am-242 and Cm-242 was evaluated as well as the combined mass of Am-243 and Cm-243. Higher mass minor actinides were not measured in detectable quantities.

The determination of burnup was performed using the measured mass of a specific fission product in the fuel, the cumulative fission yield of that specific fission product, and the total mass of actinides present in the sample. This method is sometimes referred to as the "Fission Product Monitor Residual Heavy Atom" technique [36,37]. Burnup is calculated in % fission per initial heavy metal atoms (FIMA) which is comparable to heavy metal depletion and atom % burnup units used in other sources.

$$BU = \frac{\left(N_{fp} / y_{fp} \right)}{\left(\left(N_{fp} / y_{fp} \right) + N_{Act} \right)} \times 100 \qquad (1)$$

Where N_{fp} is number of atoms of a specific fission product fp measured in the sample, y_{fp} is the cumulative fission yield of fission product fp, and N_{Act} is the number of atoms of actinides in the sample. All fission yields were taken from ENDF/B-VII.1[29]. A benefit of this burnup technique is that it requires no a priori knowledge of the sample. All the factors in Equation 1 can be directly measured from mass spectrometry results and no assumptions about the pre-irradiation state of the fuel or the size of the sampled material need to be made.

For this burnup analysis the fast fission yields were used in the calculation of burnup. The feedstock uranium in the low-fertile samples was depleted U, so U-235 fission was not considered. The burnup would be biased if only the Pu-239 cumulative fast fission yields were used in Equation (1) for burnup determination. In order to estimate the fraction of fission that occurred in a particular isotope, the effective fission yield for several isotopes was assumed to be a weighted average between the yields for Pu-239, U-238, Am-241, and Pu-240. The weighted average for each sample was determined by finding scaling weights that minimized the burnup spread among the six key fission product burnup indicators for this technique (La-139, Ce-140, Ce-142, Pr-141, Nd-145, and Nd-146). Using this minimization technique it was possible to assume that for DOE1 81% of the fission came from Pu-239 and 19% came from U-238 fast fissions, and for DOE2 all fission came from Pu-239. These assumptions are adequate for the uncertainty of the mass spectrometry data which is ±5% (2 sigma). It should be noted that there would have been some fission in the Am-241 present in both samples, but it is not possible to estimate the fraction of Am-241 fission from the available data.

There are six isotopes that work reliably for the ICP MS technique in the FUTURIX-FTA fuel: La 139, Ce 140, Ce 142, Pr 141, Nd 145, and Nd 146. These isotopes occur on the higher atomic number peak of the bimodal fission product distribution. They are all lanthanides that will readily dissolve in the selected acid. The differences between fission yields are fairly small for these isotopes as well. All these isotopes are nonradioactive and have relatively small neutron absorption cross section with the exception of Nd 145. Because of its cross section, the number of Nd 145 and Nd 146 atoms in the samples and their respective yields are summed in the calculation of burnup. In this calculation, the burnup measurement for each sample was found by taking the average of the individual isotope results from Equation (1) for La 139, Ce 140, Ce 142, Pr 141, and the Nd 145 + Nd 146 combined result. The uncertainty of all mass spectrometry values is ±5% (2 sigma), and the derived burnup values are also considered no better than 5% relative uncertainty. The measured burnup values, the measured fission densities and the burnup from simulation for each rodlet are shown in Table 4. The low fertile pin DOE1 match the simulations within 5% relative uncertainty. There is more discrepancy in the non-fertile DOE2. This is not surprising as the nuclear data associated with Pu and Am are less well known than the U data.

Table 4. Measured fission density and burnup for DOE1 and DOE2

Name	Composition*	Simulation [16] (%FIMA)	Measured Burnup (%FIMA)	Measured Fission Density (fissions/ cm^3)
DOE1	U-28.3Pu-3.8Am-2.1Np-31.7Zr	9.08%	9.53%	2.08E+21
DOE2	Pu-10.5Am-0.3Np-41.6Zr	15.50%	12.67%	2.01E+21

*Numbers preceding elements denote weight percent, subscript numbers represent mole percent. This is the as-fabricated composition not the nominal composition

5. Electron Microscopy

Only a limited amount of electron microscopy has been performed on irradiated transmutation fuels. The dose rates from full cross sections of irradiated fuels are typically too high for non-remote handling or loading into electron microscopes that are typically operated in unshielded radiological facilities. The dose rates often cause issues with the electronics in electron microscopes and their associated detectors.

Recently, it was possible to place a FUTURIX-FTA DOE1 sample shown in Figure 13 in the SEM at the INL Electron Microscopy Laboratory (EML). A montage of back-scattered electron (BSE) imaging is shown in Figure 21. In the upper right hand area of this image is some copper tape used to ground the sample electrically. In this figure, brighter areas indicate areas of higher electron density associated with higher atomic number elements. The same pore size distribution seen in the optical microscopy is also seen in the electron microscopy. The redistribution of Zr is less readily apparent than what has historically been seen in U-10Zr[4] or U-20Pu-10Zr [38], although Zr redistribution is expected to be highly composition dependent. At magnifications higher than that used for Figure 21, it is possible to observe some Zr redistribution where the Zr concentration is higher in the center of the fuel. Elsewhere in the fuel there are two observed phases throughout the fuel. One phase is a higher Zr phase that is approximately 35% U, 30% Pu, and 25% Zr. The other phase is a lower Zr, higher U phase that is approximately 60%U, 30% Pu and 10% Zr. In the mid-radius, these phases are larger (10-30µm) than the outer radius where the phases are finer (1-15µm). A higher magnification BSE image is shown in Figure 22 that details the near cladding microstructure observed throughout the fuel. Several features are indicated in Figure 22 as key features. The cladding is AIM1, which contains ~ 0.5 wt.% Ti. It appears the Ti has precipitated in the cladding during irradiation. Next to the cladding is a layer of U, Pu, Zr, Si, and possibly some Am. This layer of Si is an artifact from fabrication where Si from the quartz mold enters the fuel and was observed after fabrication [13]. The Zr layer is also an artifact from fabrication where Zr from the charge is partially stabilized by oxygen from the quartz forming a Zr rich layer. This was observed in fabrication also [13]. There are precipitates of lanthanides (La, Ce, Nd, and others) near the Zr layer. However there does not appear to be any attack of the cladding from the major fission product lanthanides (La, Ce,

Nd). The higher Zr phase and the lower Zr phase mentioned previously are also indicated. The most significant feature observed in Figure 22 is an infiltration of Am and Sm into the cladding in much the same way that lanthandies do in U-20Pu-10Zr fuel. Both of these elements have high vapor pressures. It is suspected that this infiltration is assisted by these high vapor pressures, but more research into the phenomenon is needed.

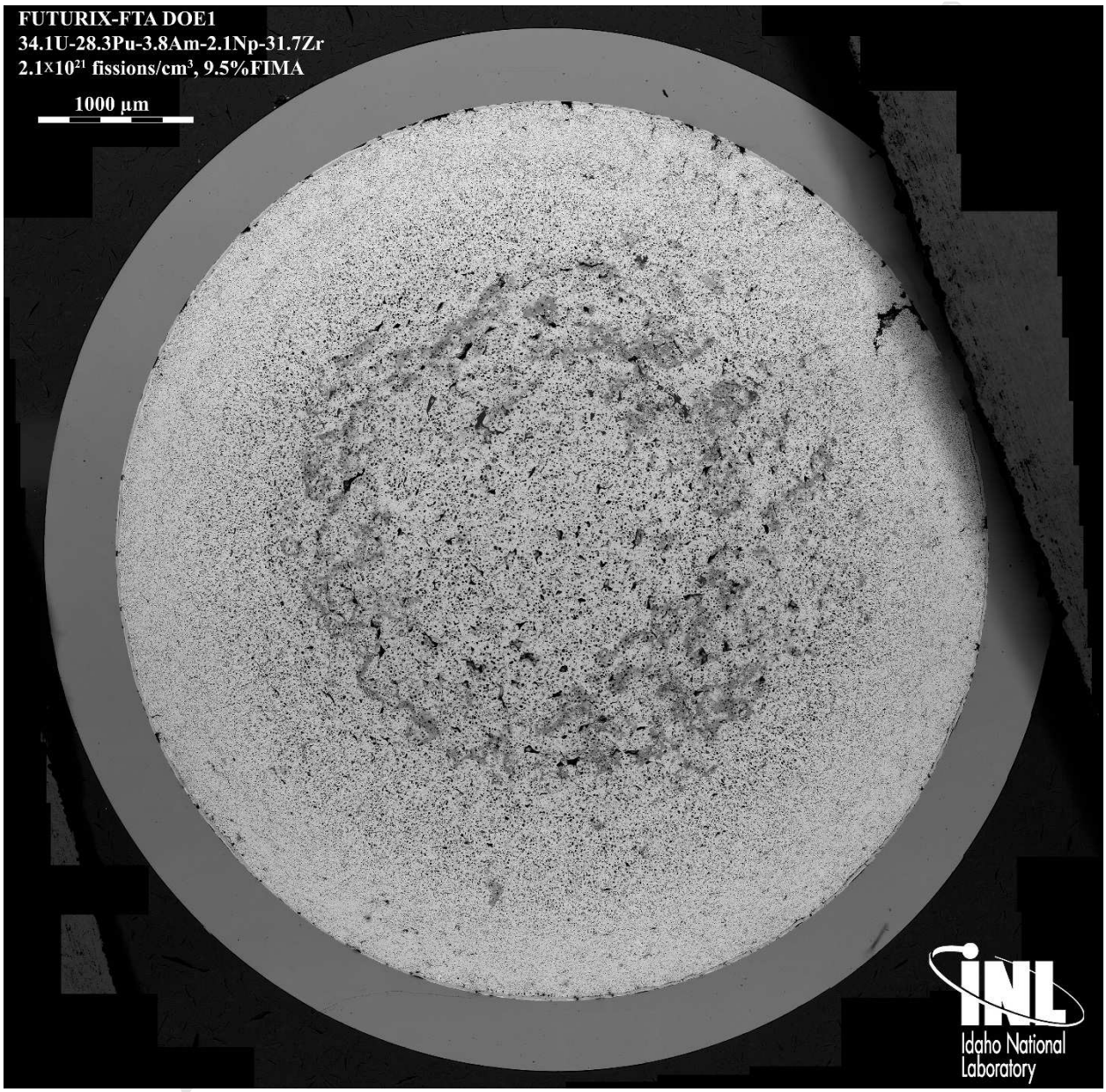

Figure 21. Back-scatter electron imaging of FUTURIX-FTA DOE1 (U-29Pu-4Am-2Np-30Zr) (low-fertile metallic).

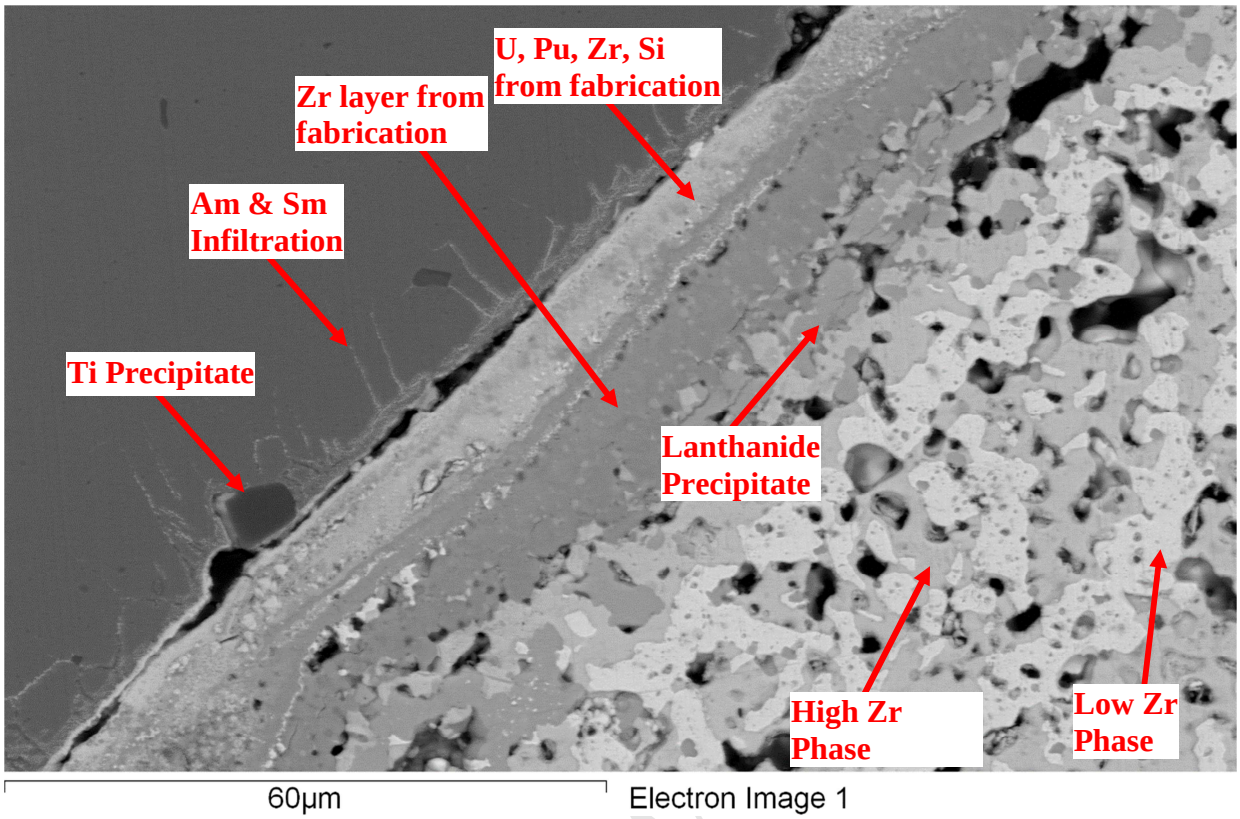

Figure 22. High magnification BSE detail of the DOE1 (low-fertile metallic) microstructure near the cladding.

6. Conclusion

The FUTURIX-FTA irradiations experiment were performed at the Phénix reactor in France as a joint collaboration between the DOE in the U.S. and the CEA in France. This program sought to develop and demonstrate the technologies needed to transmute long-lived transuranic actinide isotopes contained in spent nuclear fuel via fast reactor technology.

Irradiation tests designated FUTURIX-FTA DOE1 and FUTURIX-FTA DOE2 contain pins with low-fertile and non-fertile actinide bearing metallic alloy fuel compositions, and they were irradiated in Phénix up to burnups of 9.5 %FIMA (DOE1) and 12.7 %FIMA (DOE2).

Baseline PIE on DOE1 and DOE2 were completed at INL and reported in this work. In general, the results shows a behavior very similar to EBR-II metallic fuel experience. Minor actinides seem to not affect the general performance of this candidate transmutation fuel, despite the fuel system growing in complexity with the addition of Np, Am. Axial gamma spectrometry generally behaved as expected from literature for Cs, noble metal and lanthanide fission products. The distribution of Cs revealed by GECT suggests some

significant Na logging in DOE1. It was also possible to identify a Cm-243 signal which can be related to the distribution of Am and Cm in the fuel. Fission gas release was in-line with general expectations from the EBR-II metal fuel irradiation experience. The amount of He gas released to the fuel plenum was low compared to limited examples from literature.

The microstructure of both pins presents features that differ when compared to the well-studied U-19Pu-10Zr alloy. In DOE1, spherical porosity covered the inner 75% of the fuel cross section. This microstructure may be related to the higher content of Pu and Zr in the fuel that lowers the phase transition temperature for the high temperature cubic phase of the major elements (U,Pu,Zr). In DOE2, the microstructure appears more complex with 5 different major radial zones. The complexity of the Pu-Zr binary phase diagram coupled with the complication of a significant Am content make this observation unsurprising. The presented microscopy is the first performed on irradiated Pu-Am-Zr.

Many secondary phases / precipitates are visible throughout the fuel samples (see Figure 17 for example). Some of these are inferred to be precipitates of Am and lanthanides based on prior irradiations and SEM data on this fuel. The exact nature of these phases and the location of the Am in the fuel will require further investigation.

Other interesting results are more related to the higher contents of Pu and Zr in this fuel. Both alloys had little axial growth (0.5% for DOE1 and 3% for DOE2) and diametral strain (quantified in 0.1%) compared to U-19Pu-10Zr. These features might be an indication that higher Zr content and the absence of U in DOE2 might limit the anisotropic growth and high swelling behavior of alpha-U.

More extensive SEM examinations and electron microprobe analyzer (EPMA) examinations are required to more fully quantify the major and minor phases present. Micro-XRD and the preparation of transmission (TEM) lamella by Focused Ion Beam (FIB) would also be helpful to fully understand this system.

Disclosure statement

This manuscript has been authored by Battelle Energy Alliance, LLC under Contract No. DE-AC07-05ID14517 with the U.S. Department of Energy. The United States Government retains and the publisher, by accepting the article for publication, acknowledges that the

Acknowledgements

This work was supported by the U.S. Department of Energy, Advanced Fuels Campaign of the Nuclear Technology Research and Development program in the Office of Nuclear Energy.

References

[1] S.L. Hayes, B.A. Hilton, M.K. Meyer, G.S. Chang, F.W. Ingram, S. Pillon, N. Schmidt, L. Leconte, D. Haas, U.S. Test Plans for Actinide Transmutation Fuel Development, in: Trans. Am. Nucl. Soc. Vol. 87, 2002: p. 353.

[2] Report to Congress on the Advanced Fuel Cycle Initiative: The Future Path for Advanced Spent Fuel Treatment and Transmutation Research, (2003).

[3] G.L. Hofman, L.C. Walters, T.H. Bauer, Metallic fast reactor fuels, Prog. Nucl. Energy. 31 (1997) 83–110. doi:10.1016/0149-1970(96)00005-4.

[4] G.L. Hofman, S.L. Hayes, M.C. Petri, Temperature gradient driven constituent redistribution in U□Zr alloys, J. Nucl. Mater. 227 (1996) 277–286. doi:10.1016/0022-3115(95)00129-8.

[5] D.C. Crawford, D.L. Porter, S.L. Hayes, Fuels for sodium-cooled fast reactors: US perspective, J. Nucl. Mater. 371 (2007) 202–231. doi:10.1016/J.JNUCMAT.2007.05.010.

[6] W.J. Carmack, D.L. Porter, Y.I. Chang, S.L. Hayes, M.K. Meyer, D.E. Burkes, C.B. Lee, T. Mizuno, F. Delage, J. Somers, Metallic fuels for advanced reactors, J. Nucl. Mater. 392 (2009) 139–150. doi:10.1016/J.JNUCMAT.2009.03.007.

[7] T. Ogata, Metal Fuel, in: Compr. Nucl. Mater., Elsevier, 2012: pp. 1–40. doi:10.1016/B978-0-08-056033-5.00049-5.

[8] H. Ohta, T. Ogata, D. Papaioannou, V. V Rondinell, M. Masson, J.-L. Paul, Irradiation of Minor Actinide–Bearing Uranium-Plutonium-Zirconium Alloys up to ˜2.5 at. %, ˜7 at. %, and ˜10 at. % Burnups, Nucl. Technol. 190 (2015) 36–51. doi:10.13182/NT14-50.

[9] L. Capriotti, S. Brémier, K. Inagaki, P. Pöml, D. Papaioannou, H. Ohta, T. Ogata, V.V. Rondinella, Characterization of metallic fuel for minor actinides transmutation in fast

reactor, Prog. Nucl. Energy. 94 (2017) 194–201. doi:10.1016/J.PNUCENE.2016.04.004.

[10] J.H. Kim, H. Song, K.H. Kim, C.B. Lee, Fabrication and evaluation of rare-earth-bearing fuel slugs for sodium-cooled fast reactors, J. Radioanal. Nucl. Chem. 303 (2015) 615–621. doi:10.1007/s10967-014-3513-3.

[11] N. Chauvin, K. Minato, T. Ogata, C.B. Lee, M.A. Pouchon, K.O. Pasamehmetoglu, Y.J. Choi, J.R. Kennedy, S. Massara, S. Cornet, J. Sommers, K. McClellan, State-of-the-art Report on Innovative Fuels for Advanced Nuclear Systems, OECD, NEA No. 6895. (2014). https://inis.iaea.org/search/search.aspx?orig_q=RN:46027255 (accessed August 9, 2018).

[12] J.M. Harp, H.J.M. Chichester, L. Capriotti, Baseline Postirradiation Examination of the FUTURIX FTA Experiment, Idaho Natl. Lab. Rep. (2016) INL/LTD-16-40088.

[13] J.R. Kennedy, FUTURIX-FTA Metal Alloy Fuel Fabrication and Characterization Report, Idaho Natl. Lab. Rep. (2007) INL/EXT-07-12234.

[14] J.S. Cheon, C.B. Lee, B.O. Lee, J.P. Raison, T. Mizuno, F. Delage, J. Carmack, Sodium fast reactor evaluation: Core materials, J. Nucl. Mater. 392 (2009) 324–330. doi:10.1016/J.JNUCMAT.2009.03.021.

[15] P. Gavoille, A. Courcelle, J.L. Seran, X. Averty, B. Bourdiliau, O. Provitina, V. Garat, D. Verwaerde, Mechanical Properties of Cladding and Wrapper Materials for the ASTRID Fast-Reactor Project, in: IAEA Int. Conf. Fast React. Relat. Fuel Cycles Safe Technol. Sustain. Scenar., 2013. https://inis.iaea.org/search/search.aspx?orig_q=RN:45089554.

[16] I. Munoz, C. Repetto, B. Valentin, Irradiation Report of the FUTURIX-FTA Metal Capsule, Commis. à l'Energie At. Aux Energies Altern. Rep. (2014) CEA Cadarache, CEA/DEN/CAD/DEC/SESC/LC2I NT 12-020.

[17] A.E. Craft, D.M. Wachs, M.A. Okuniewski, D.L. Chichester, W.J. Williams, G.C. Papaioannou, A.T. Smolinski, Neutron Radiography of Irradiated Nuclear Fuel at Idaho National Laboratory, Phys. Procedia. 69 (2015) 483–490. doi:10.1016/J.PHPRO.2015.07.068.

[18] G.L. Hofman, Irradiation Behavior of Experimental Mark-II Experimental Breeder Reactor II Driver Fuel, Nucl. Technol. 47 (1980) 7–22. doi:10.13182/NT80-A32408.

[19] D.E. Burkes, R.S. Fielding, D.L. Porter, D.C. Crawford, M.K. Meyer, A US perspective on fast reactor fuel fabrication technology and experience part I: metal fuels and assembly design, J. Nucl. Mater. 389 (2009) 458–469. doi:10.1016/J.JNUCMAT.2009.02.035.

[20] D.L. Porter, G.L. Hofman, B.R. Seidel, L.C. Walters, Factors controlling metal fuel lifetime, in: Int. Conf. Reliab. Fuels Liq. Met. Factors, Tuscon, AZ, 1986. https://www.osti.gov/biblio/6891881-factors-controlling-metal-fuel-lifetime.

[21] D.L. Porter, H. Tsai, Full-length U–xPu–10Zr (x = 0, 8, 19 wt.%) fast reactor fuel test in FFTF, J. Nucl. Mater. 427 (2012) 46–57. doi:10.1016/J.JNUCMAT.2012.03.047.

[22] R.G. Pahl, R.S. Wisner, M.C. Billone, G.L. Hofman, Steady-state irradiation testing of U-Pu-Zr fuel to >18% burnup, in: Conf. Int. Top. Meet. Fast React. Saf., Snow Bird, Utah,United States, 1990. https://www.osti.gov/servlets/purl/7177201.

[23] J.M. Harp, J.W. Sterbentz, P.A. Demkowicz, P.L. Winston, R.P. Lind, Examination of individual compact burnup for the AGR-1 TRISO fuel experiment using gamma spectrometry, in: Trans. Am. Nucl. Soc., 2011.

[24] J.M. Harp, P.A. Demkowicz, Investigation of the Feasibility of Utilizing Gamma Emission Computed Tomography in Evaluating Fission Product Migration in Irradiated TRISO Fuel Experiments, in: Int. Top. Meet. High Temp. React. Technol. (HTR 2014), WeiHai, China, 2014.

[25] J.D. Hunn, C.A. Baldwin, T.J. Gerczak, F.C. Montgomery, R.N. Morris, C.M. Silva, P.A. Demkowicz, J.M. Harp, S.A. Ploger, Detection and analysis of particles with failed SiC in AGR-1 fuel compacts, Nucl. Eng. Des. (2015). doi:10.1016/j.nucengdes.2015.12.011.

[26] J.M. Harp, H.J.M. Chichester, L. Capriotti, Postirradiation examination results of several metallic fuel alloys and forms from low burnup AFC irradiations, J. Nucl. Mater. 509 (2018) 377–391. doi:10.1016/J.JNUCMAT.2018.07.003.

[27] Personal Communication, Douglas C. Porter, EBR-II X-419 PIE archive data, (1985).

[28] J.M. Harp, L. Capriotti, H.J.M. Chichester, P.G. Medvedev, D.L. Porter, S.L. Hayes, Postirradiation examination on metallic fuel in the AFC-2 irradiation test series, J. Nucl. Mater. (2018). doi:10.1016/J.JNUCMAT.2018.07.019.

[29] M.B. Chadwick, M. Herman, P. Obložinský, M.E. Dunn, Y. Danon, A.C. Kahler, D.L. Smith, B. Pritychenko, G. Arbanas, R. Arcilla, R. Brewer, D.A. Brown, R. Capote, A.D. Carlson, Y.S. Cho, H. Derrien, K. Guber, G.M. Hale, S. Hoblit, S. Holloway, T.D. Johnson, T. Kawano, B.C. Kiedrowski, H. Kim, S. Kunieda, N.M. Larson, L. Leal, J.P. Lestone, R.C. Little, E.A. McCutchan, R.E. MacFarlane, M. MacInnes, C.M. Mattoon, R.D. McKnight, S.F. Mughabghab, G.P.A. Nobre, G. Palmiotti, A. Palumbo, M.T. Pigni, V.G. Pronyaev, R.O. Sayer, A.A. Sonzogni, N.C. Summers, P. Talou, I.J. Thompson, A. Trkov, R.L. Vogt, S.C. van der Marck, A. Wallner, M.C. White, D. Wiarda, P.G. Young, ENDF/B-VII.1 Nuclear Data for Science and Technology: Cross Sections, Covariances, Fission Product Yields and Decay Data, Nucl. Data Sheets. 112 (2011) 2887–2996. doi:10.1016/J.NDS.2011.11.002.

[30] B. Hilton, D. Porter, S. Hayes, AFC-1 Transmutation Fuels Post-Irradiation Hot Cell Examination 4-8 at.% - Final Report (Irradiation Experiments AFC-1B, -1F and -1Æ), Idaho Natl. Lab. Rep. (2006) INL/EXT-05-00785. doi:10.2172/911779.

[31] H.J.M. Chichester, D.L. Porter, B.A. Hilton, Postirradiation Examination of AFC-1D, 1G, 1H, and 2A Experiments, Idaho Natl. Lab. Rep. (2011) INL/LTD-11-23242.

[32] J.M. Harp, S.L. Hayes, P.G. Medvedev, D.L. Porter, L. Capriotti, Testing Fast Reactor Fuels in a Thermal Reactor: A Comparison Report, Idaho Natl. Lab. Rep. (2017) INL/EXT-17-41677. doi:10.2172/1458766.

[33] M.K. Meyer, S.L. Hayes, W.J. Carmack, H. Tsai, The EBR-II X501 minor actinide burning experiment, J. Nucl. Mater. 392 (2009) 176–183. doi:10.1016/J.JNUCMAT.2009.03.041.

[34] D.E. Janney, Metallic Fuels Handbook, Idaho National Laboratory Report, INL/EXT-15-36520 r2, 2017. doi:10.2172/1392980.

[35] J.M. Harp, D.L. Porter, B.D. Miller, T.L. Trowbridge, W.J. Carmack, Scanning electron microscopy examination of a Fast Flux Test Facility irradiated U-10Zr fuel cross section clad with HT-9, J. Nucl. Mater. 494 (2017) 227–239. doi:10.1016/j.jnucmat.2017.07.040.

[36] W.J. Maeck, R.P. Larsen, J.E. Rein, Burnup Determination for Fast Reactor Fuels: A Review and Status of the Nuclear Data and Analytical Chemistry Methodology Requirements, U.S. At. Energy Comm. TID-26209 (1973).

[37] J.M. Harp, P.A. Demkowicz, P.L. Winston, J.W. Sterbentz, An analysis of nuclear fuel burnup in the AGR-1 TRISO fuel experiment using gamma spectrometry, mass spectrometry, and computational simulation techniques, Nucl. Eng. Des. 278 (2014) 395–405. doi:10.1016/j.nucengdes.2014.07.041.

[38] Y.S. Kim, G.. Hofman, S.. Hayes, Y.. Sohn, Constituent redistribution in U–Pu–Zr fuel during irradiation, J. Nucl. Mater. 327 (2004) 27–36. doi:10.1016/J.JNUCMAT.2004.01.012.